

A common lines approach for ab-initio modeling of cyclically-symmetric molecules

Gabi Pragier and Yoel Shkolnisky

Department of Applied Mathematics, School of Mathematical Sciences, Tel-Aviv University, Israel

Abstract

One of the challenges in single particle reconstruction in cryo-electron microscopy is to find a three-dimensional model of a molecule using its two-dimensional noisy projection-images. In this paper, we propose a robust “angular reconstitution” algorithm for molecules with n -fold cyclic symmetry, that estimates the orientation parameters of the projections-images. Our suggested method utilizes self common lines which induce identical lines within the Fourier transform of each projection-image. We show that the location of self common lines admits quite a few favorable geometrical constraints, thus allowing to detect them even in a noisy setting. In addition, for molecules with higher order rotational symmetry, our proposed method exploits the fact that there exist numerous common lines between any two Fourier transformed projection-images of such molecules, thus allowing to determine their relative orientation even under high levels of noise. The efficacy of our proposed method is demonstrated using numerical experiments conducted on simulated and experimental data.

1. Introduction

Cryo-electron microscopy is a method for determining the three-dimensional structure of a molecule from its two-dimensional projection-images [3]. The method consists of generating projection-images of copies of the investigated molecule, where each copy assumes a random unknown orientation before being imaged. Formally, if we denote by $\psi: \mathbb{R}^3 \rightarrow \mathbb{R}$ the electrostatic potential of the molecule, and consider a

Email address: gabipragier@gmail.com, yoelsh@tauex.tau.ac.il (Gabi Pragier and Yoel Shkolnisky)

rotation matrix

$$SO(3) \ni R_i = \begin{pmatrix} \left| \begin{array}{c} R_i^{(1)} \\ \hline \end{array} \right. & \left| \begin{array}{c} R_i^{(2)} \\ \hline \end{array} \right. & \left| \begin{array}{c} R_i^{(3)} \\ \hline \end{array} \right. \end{pmatrix}, \quad (1)$$

then the projection-image P_{R_i} is given by the line integrals of ψ along the beaming-direction $R_i^{(3)}$. That is,

$$P_{R_i}(x, y) = \int_{-\infty}^{\infty} \psi(R_i r) dz = \int_{-\infty}^{\infty} \psi(xR_i^{(1)} + yR_i^{(2)} + zR_i^{(3)}) dz, \quad r = (x, y, z)^T. \quad (2)$$

In this work, we focus on molecules that have an n -fold, $n \geq 2$, rotational symmetry about some unknown axis. Such molecules are referred to as molecules with C_n symmetry. We assume that the cyclic symmetry order n of the underlying molecule is known from prior knowledge, or may be inferred from rotational invariants computed by spherical harmonics (see e.g., [7]). Intuitively, molecules with C_n symmetry “look exactly the same” when rotated by $2\pi s/n$, $s \in [n-1]$ (we subsequently denote by $[m]$ the set $\{1, \dots, m\}$), radians about their axis of symmetry. Mathematically, it means that the electrostatic potential function $\psi: \mathbb{R}^3 \rightarrow \mathbb{R}$ of any such molecule satisfies

$$\psi(r) = \psi(g_n r) = \dots = \psi(g_n^{n-1} r), \quad \forall r \in \mathbb{R}^3, \quad (3)$$

where $g_n \in SO(3)$ represents a rotation of $2\pi/n$ radians about the unknown axis of symmetry, and $n \in \mathbb{N}$ is the largest for which (3) holds. Since rotating the three-dimensional coordinate system has no effect on the three-dimensional structure of the molecule, it may be assumed without loss of generality that the axis of symmetry coincides with the z -axis. Thus, the matrix g_n which satisfies (3) may be written as

$$g_n = \begin{pmatrix} \cos(2\pi/n) & -\sin(2\pi/n) & 0 \\ \sin(2\pi/n) & \cos(2\pi/n) & 0 \\ 0 & 0 & 1 \end{pmatrix}, \quad (4)$$

and any three-dimensional coordinate system for the molecule must be set such that it keeps the axis of symmetry aligned with the z -axis (with possibly flipping its orientation). That is, the degrees of freedom in setting the three-dimensional coordinate system of the molecule consist of in-plane rotations about the z -axis, and an in-plane rotation of π radians about either the x -axis or the y -axis.

Finding the three-dimensional structure of the molecule amounts to recovering the unknown electrostatic potential function ψ given only the projection-images P_{R_i} .

Typically, this is done by first finding the rotation matrices R_i , followed by a standard tomographic inversion algorithm e.g., [5, 11].

A fundamental limitation of cryo-electron microscopy is the handedness ambiguity [14], whereby the best one may expect is to recover either the set $\{R_i\}_{i=1}^m$ or the set $\{R_i J\}_{i=1}^m$ where $J = \text{diag}(-1, -1, 1)$, not being able to distinguish between the two. Indeed, given any molecule whose electrostatic potential function is ψ , consider the molecule whose electrostatic potential function $\tilde{\psi}$ is given by $\tilde{\psi}(r) = \psi(-r)$, $r \in \mathbb{R}^3$. For any R_i , the projection-image $\tilde{P}_{R_i J}$ of the molecule $\tilde{\psi}$ is given according to (2) by

$$\tilde{P}_{R_i J}(x, y) = \int_{-\infty}^{\infty} \tilde{\psi}(R_i J r) dz = \int_{-\infty}^{\infty} \psi(-R_i J r) dz, \quad (5)$$

where $r = (x, y, z)^T \in \mathbb{R}^3$. Noting that $-Jr = (x, y, -z)$, and by changing the variable z to $z' = -z$ we have

$$\int_{-\infty}^{\infty} \psi(-R_i J r) dz = \int_{-\infty}^{\infty} \psi(R_i (x, y, z')^T) dz' = P_{R_i}(x, y). \quad (6)$$

As such, both $\{R_i\}_{i=1}^m$ and $\{R_i J\}_{i=1}^m$ are consistent with the same set of projection-images $\{P_{R_i}\}_{i=1}^m$, yet the reconstructed model using the latter set is biologically infeasible, and the true set may therefore only be determined by visual examination of the reconstructed model, possibly exploiting other known structural information. Furthermore, an important property of molecules with C_n symmetry is that any n projection-images $P_{R_i}, P_{g_n R_i}, \dots, P_{g_n^{n-1} R_i}$, $i \in [m]$, are identical. Indeed, from (3)

$$\psi(R_i r) = \psi(g_n R_i r) = \dots = \psi(g_n^{n-1} R_i r) \quad \forall r \in \mathbb{R}^3. \quad (7)$$

Thus, by letting $r = (x, y, z)^T$, and integrating over z , it follows from (2) that for any $s \in [n-1]$,

$$P_{g_n^s R_i}(x, y) = \int_{-\infty}^{\infty} \psi(g_n^s R_i r) dz = \int_{-\infty}^{\infty} \psi(R_i r) dz = P_{R_i}(x, y). \quad (8)$$

Equations (5), (6), and (8) show that for each R_i in the forward imaging model (2) there exists an equivalence class $\mathcal{R}_i = \{O g_n^{s_i} R_i J^\delta\}$, with $s_i \in [n]$, $O \in SO(3)$, and $\delta \in \{0, 1\}$, such that $P_{R_i} = P_{R_i^*}$ for any $R_i^* \in \mathcal{R}_i$. The matrices $g_n^{s_i}$ are due to the ambiguity stated in (7) and so s_i may be chosen independently for each image $i = 1, \dots, m$, while δ and $O \in SO(3)$ are common to all images, with O being some in-plane rotation matrix about the z -axis (the axis of symmetry). In other words,

there are no “true” rotation matrices R_i that need to be recovered, as may be implied from (2), but rather we need to recover for each $i = 1, \dots, m$ any member of the equivalence class \mathcal{R}_i . In summary, in light of the above, given projection-images $\{P_{R_i}\}_{i=1}^m$ of a molecule with C_n symmetry, the goal is to recover m rotation matrices $\{Og_n^{s_i}R_iJ^\delta\}_{i=1}^m$, where $s_i \in [n]$, $O \in SO(3)$, and $\delta \in \{0, 1\}$, such that (2) is satisfied for all $i \in [m]$ for some $\psi: \mathbb{R}^3 \rightarrow \mathbb{R}$.

The rest of this paper is organized as follows. In Sections 2 and 3 we review the projection slice theorem [10] and further describe the properties of common lines and self common lines which are induced by this theorem. In Section 4 we review some previous work. In Section 5 we present an outline of our proposed method. Next, in Section 6, we describe how to estimate the third row of each rotation matrix R_i . A procedure that assures that all these estimates correspond to a single hand (see Section 1 which points out the inherent handedness ambiguity in cryo-electron microscopy) is presented in Section 7. In Section 8 we then describe a method to determine the remaining first two rows of each R_i . Then, in Section 9 we report some numerical experiments that we conducted on simulated and experimental datasets that show the efficacy of our proposed method. Finally, in Section 10 we present some conclusions and possible extensions of this work.

As the cases of C_3 and C_4 symmetry exhibit special geometry which is advantageous from the computational point-of-view, we describe in Appendix A an algorithm for estimating the third row of each rotation matrix R_i for molecules with such symmetries. This algorithm may replace the algorithm of Section 6 for such symmetries, as it is much faster and is empirically observed to be more robust to noise. Unfortunately, generalizations of the geometry derived in Appendix A for C_n with $n > 4$ are of little practical use.

2. Common lines

The projection slice theorem [10] is a key theorem underpinning many of the methods for recovering the rotation matrices of a given set of projection-images. It states that the two-dimensional Fourier transform of any projection-image P_{R_i} is equal to the restriction of the three-dimensional Fourier transform of the electrostatic potential function ψ to the central plane $\mathcal{T}_{R_i} = \text{span}\{R_i^{(1)}, R_i^{(2)}\} \subset \mathbb{R}^3$, whose normal coincides with $R_i^{(3)}$ (the third column of R_i of (1)). Mathematically, if we denote by $\hat{\psi}$ the three-dimensional Fourier transform of ψ , and denote by \hat{P}_{R_i} the two-dimensional Fourier transform of the projection-image P_{R_i} , then the projection slice

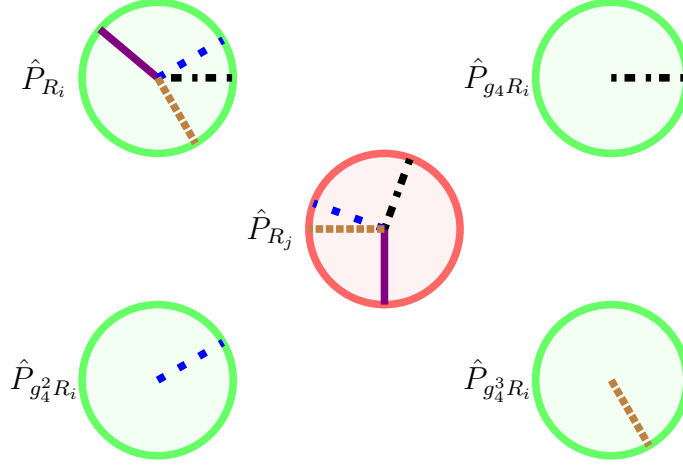


Figure 1: An illustration of Lemma 2.1 for the case of C_4 . The red circle corresponds to some image \hat{P}_{R_j} . The four green circles correspond to some other four identical images $\hat{P}_{R_i}, \hat{P}_{g_4 R_i}, \hat{P}_{g_4^2 R_i}, \hat{P}_{g_4^3 R_i}$. The lines in \hat{P}_{R_i} and \hat{P}_{R_j} represent their four common lines, each of which is induced by a common line between \hat{P}_{R_j} and one of the images $\hat{P}_{R_i}, \hat{P}_{g_4 R_i}, \hat{P}_{g_4^2 R_i}, \hat{P}_{g_4^3 R_i}$.

theorem states that

$$\hat{P}_{R_i}(\omega_x, \omega_y) = \hat{\psi}(R_i \omega), \quad \forall \omega = (\omega_x, \omega_y, 0)^T \in \mathbb{R}^3. \quad (9)$$

As such, since any two central planes \mathcal{T}_{R_i} and \mathcal{T}_{R_j} which are not parallel intersect along a common axis, it follows that any two Fourier-transformed images \hat{P}_{R_i} and \hat{P}_{R_j} have a pair of lines (one line in each image) on which their values agree. Such pairs of lines are called “common lines”. Hereafter we refer to \hat{P}_{R_i} and \hat{P}_{R_j} simply as “images”. The following lemma shows that any two images of a molecule with C_n symmetry have n pairs of common lines (see Figure 1 for an illustration of the case $n = 4$).

Lemma 2.1. *For any two images \hat{P}_{R_i} and \hat{P}_{R_j} , such that $\left| \left\langle R_i^{(3)}, R_j^{(3)} \right\rangle \right| \neq 1$, there exist angles $\alpha_{ij}^{(s)}, \alpha_{ji}^{(s)} \in [0, 2\pi)$, $s = 0, \dots, n-1$, such that for any $\xi \in \mathbb{R}$,*

$$\hat{P}_{R_i}(\xi \cos \alpha_{ij}^{(s)}, \xi \sin \alpha_{ij}^{(s)}) = \hat{P}_{R_j}(\xi \cos \alpha_{ji}^{(s)}, \xi \sin \alpha_{ji}^{(s)}). \quad (10)$$

Proof. Denote by $q_{ij}^{(s)} \in \mathbb{R}^3$, $s = 0, \dots, n-1$, the unit vector in the direction of the

common axis between \mathcal{T}_{R_i} and $\mathcal{T}_{g_n^s R_j}$, namely

$$q_{ij}^{(s)} = \frac{R_i^{(3)} \times g_n^s R_j^{(3)}}{\|R_i^{(3)} \times g_n^s R_j^{(3)}\|}, \quad s = 0, \dots, n-1. \quad (11)$$

Also denote for every $s = 0, \dots, n-1$

$$\begin{aligned} \left(\cos \alpha_{ij}^{(s)}, \sin \alpha_{ij}^{(s)}, 0 \right)^T &= R_i^T q_{ij}^{(s)}, \\ \left(\cos \alpha_{ji}^{(s)}, \sin \alpha_{ji}^{(s)}, 0 \right)^T &= (g_n^s R_j)^T q_{ij}^{(s)}. \end{aligned} \quad (12)$$

That is, the angles $\alpha_{ij}^{(s)}$ and $\alpha_{ji}^{(s)}$ express $q_{ij}^{(s)}$ in the frame of reference of \mathcal{T}_{R_i} and in the frame of reference $\mathcal{T}_{g_n^s R_j}$, respectively. Now, by (7), (9) and (12), for $\xi \in \mathbb{R}$ and $s = 0, \dots, n-1$,

$$\begin{aligned} \hat{P}_{R_i} \left(\xi \cos \alpha_{ij}^{(s)}, \xi \sin \alpha_{ij}^{(s)} \right) &= \hat{\psi} \left(\xi q_{ij}^{(s)} \right) = \hat{\psi} \left(\xi g_n^{-s} q_{ij}^{(s)} \right) \\ &= \hat{\psi} \left(\xi R_j R_j^T g_n^{-s} q_{ij}^{(s)} \right) = \hat{\psi} \left(\xi R_j (g_n^s R_j)^T q_{ij}^{(s)} \right) \\ &= \hat{P}_{R_j} \left(\xi \cos \alpha_{ji}^{(s)}, \xi \sin \alpha_{ji}^{(s)} \right). \end{aligned} \quad (13)$$

□

The relative orientation between any two central planes \mathcal{T}_{R_i} and $\mathcal{T}_{g_n^s R_j}$ is expressed algebraically by $R_i^T g_n^s R_j$ (henceforth regarded as the relative orientation between \mathcal{T}_{R_i} and $\mathcal{T}_{g_n^s R_j}$). In addition, denoting by $\gamma_{ij}^{(s)}$, $s \in [n]$, the acute angle between the central planes \mathcal{T}_{R_i} and $\mathcal{T}_{g_n^s R_j}$, we get that $(\alpha_{ij}^{(s)}, \gamma_{ij}^{(s)}, -\alpha_{ji}^{(s)})$ is the “ x -convention” Euler angles parameterization [17] of $R_i^T g_n^s R_j$. Specifically,

$$R_i^T g_n^s R_j = R_z(\alpha_{ij}^{(s)}) R_x(\gamma_{ij}^{(s)}) R_z(-\alpha_{ji}^{(s)}), \quad (14)$$

where

$$R_x(\theta) = \begin{pmatrix} 1 & 0 & 0 \\ 0 & \cos \theta & -\sin \theta \\ 0 & \sin \theta & \cos \theta \end{pmatrix} \quad \text{and} \quad R_z(\theta) = \begin{pmatrix} \cos \theta & -\sin \theta & 0 \\ \sin \theta & \cos \theta & 0 \\ 0 & 0 & 1 \end{pmatrix} \quad (15)$$

denote the matrices that rotate vectors by $\theta \in \mathbb{R}$ radians about the x -axis and z -axis,

respectively. Finally, we mention in passing that any $\alpha_{ij}^{(s)}$ and $\alpha_{ji}^{(s)}$ may be recovered from the entries of $R_i^T g_n^s R_j$ using (see [15])

$$\alpha_{ij}^{(s)} = \arctan \left(-\frac{(R_i^T g_n^s R_j)_{1,3}}{(R_i^T g_n^s R_j)_{2,3}} \right), \quad \alpha_{ji}^{(s)} = \arctan \left(-\frac{(R_i^T g_n^s R_j)_{3,1}}{(R_i^T g_n^s R_j)_{3,2}} \right). \quad (16)$$

3. Self common lines

A “self common line” is a common line between any two images \hat{P}_{R_i} and $\hat{P}_{g_n^s R_i}$ with $s \in [n-1]$. Thus, similarly to (10), for any $i \in [m]$ there exist angles $\alpha_{ii}^{(s)}, \alpha_{gi}^{(s)} \in [0, 2\pi)$, $s = 1, \dots, n-1$ (the subscripts will be clarified shortly), such that for any $\xi \in \mathbb{R}$

$$\hat{P}_{R_i} \left(\xi \cos \alpha_{ii}^{(s)}, \xi \sin \alpha_{ii}^{(s)} \right) = \hat{P}_{g_n^s R_i} \left(\xi \cos \alpha_{gi}^{(s)}, \xi \sin \alpha_{gi}^{(s)} \right).$$

Since by (8), any two such images \hat{P}_{R_i} and $\hat{P}_{g_n^s R_i}$ are identical, it follows that

$$\hat{P}_{R_i} \left(\xi \cos \alpha_{ii}^{(s)}, \xi \sin \alpha_{ii}^{(s)} \right) = \hat{P}_{R_i} \left(\xi \cos \alpha_{gi}^{(s)}, \xi \sin \alpha_{gi}^{(s)} \right), \quad i \in [m], s \in [n-1]. \quad (17)$$

That is, any image \hat{P}_{R_i} has $n-1$ pairs of identical lines (regarded henceforth as self common lines as well). Similarly to (12), the angles $\alpha_{ii}^{(s)}$ and $\alpha_{gi}^{(s)}$ may be expressed in terms of the unit vector $q_{ii}^{(s)} \in \mathbb{R}^3$ of (11) in the direction of the common axis between the central planes \mathcal{T}_{R_i} and $\mathcal{T}_{g_n^s R_i}$ as

$$\begin{aligned} \left(\cos \alpha_{ii}^{(s)}, \sin \alpha_{ii}^{(s)}, 0 \right)^T &= R_i^T q_{ii}^{(s)}, \\ \left(\cos \alpha_{gi}^{(s)}, \sin \alpha_{gi}^{(s)}, 0 \right)^T &= (g_n^s R_i)^T q_{ii}^{(s)}. \end{aligned} \quad (18)$$

The following lemma shows that the direction of the s -th and the $(n-s)$ -th pairs of self common lines in any image coincide.

Lemma 3.1. *For any $i \in [m]$, and for any $s \in [n-1]$,*

$$\alpha_{gi}^{(s)} = \alpha_{ii}^{(n-s)} + \pi \pmod{2\pi}. \quad (19)$$

The proof of Lemma 3.1 is given in Appendix B.1. Figure 2a and Figure 2b illustrate Lemma 3.1 for C_3 and C_4 symmetries, respectively.

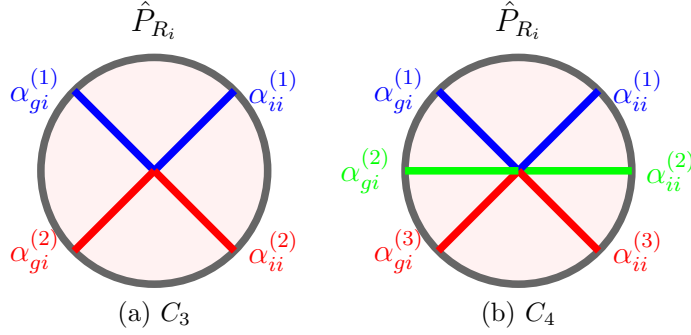


Figure 2: Circles representing an image \hat{P}_{R_i} of a molecule with C_3 symmetry (left) and of a molecule with C_4 symmetry (right), along with the pairs of self common lines in each image. By Lemma 3.1 the lines are collinear.

Corollary 3.2. *By (17) and (19) it follows that for any $i \in [m]$, $s \in [n - 1]$, and $\xi \in \mathbb{R}$,*

$$\begin{aligned} \hat{P}_{R_i} \left(\xi \cos \alpha_{ii}^{(s)}, \xi \sin \alpha_{ii}^{(s)} \right) &= \hat{P}_{R_i} \left(\xi \cos \alpha_{gi}^{(s)}, \xi \sin \alpha_{gi}^{(s)} \right) \\ &= \hat{P}_{R_i} \left(\xi \cos(\alpha_{ii}^{(n-s)} + \pi), \xi \sin(\alpha_{ii}^{(n-s)} + \pi) \right). \end{aligned} \quad (20)$$

In addition, as \hat{P}_{R_i} is conjugate-symmetric (since P_{R_i} is real-valued (2)),

$$\hat{P}_{R_i} \left(\xi \cos(\alpha_{ii}^{(n-s)} + \pi), \xi \sin(\alpha_{ii}^{(n-s)} + \pi) \right) = \overline{\hat{P}_{R_i} \left(\xi \cos \alpha_{ii}^{(n-s)}, \xi \sin \alpha_{ii}^{(n-s)} \right)}, \quad (21)$$

where $\overline{(\cdot)}$ denotes complex conjugation. As a result,

$$\hat{P}_{R_i} \left(\xi \cos \alpha_{ii}^{(s)}, \xi \sin \alpha_{ii}^{(s)} \right) = \overline{\hat{P}_{R_i} \left(\xi \cos \alpha_{ii}^{(n-s)}, \xi \sin \alpha_{ii}^{(n-s)} \right)}, \quad \forall \xi \in \mathbb{R}. \quad (22)$$

We therefore see from Lemma 3.1 and Corollary 3.2 that the $n - 1$ pairs of self common lines in any image consist in fact of $\lfloor \frac{n-1}{2} \rfloor$ different pairs. In addition, in case n is even, the two self common lines that constitute the $\frac{n}{2}$ -th pair of lines are collinear. In particular, for molecules with C_2 symmetry, the sole pair of self common lines in any image consists of two collinear lines. In contrast,

- for molecules with C_3 symmetry (i.e., $n = 3$), the two pairs of self common lines (i.e., four lines altogether) in any image coincide (i.e., there are merely two non-collinear lines), see Figure 2a,

- for molecules with C_4 symmetry (i.e., $n = 4$), one of the pairs of self common lines in every image consists of collinear lines whereas the other two remaining pairs of self common lines coincide, see Figure 2b, and
- for molecules with cyclic symmetry of higher order (i.e., C_n , $n > 4$), each image has in general $\lfloor \frac{n-1}{2} \rfloor > 1$ pairs of non-collinear self common lines.

In what follows, we refer to any relative orientation $R_i^T g_n^s R_i$, $i \in [m]$, $s \in [n - 1]$, as the self relative orientation between \mathcal{T}_{R_i} and $\mathcal{T}_{g_n^s R_i}$. By (14), any such self relative orientation is parameterized by the ordered triplet $(\alpha_{ii}^{(s)}, \gamma_{ii}^{(s)}, -\alpha_{gi}^{(s)})$ which by Lemma 3.1 is equal to $(\alpha_{ii}^{(s)}, \gamma_{ii}^{(s)}, -\alpha_{ii}^{(n-s)} - \pi)$. As such,

$$R_i^T g_n^s R_i = R_z(\alpha_{ii}^{(s)}) R_x(\gamma_{ii}^{(s)}) R_z(-\alpha_{ii}^{(n-s)} - \pi), \quad (23)$$

where, by (16),

$$\alpha_{ii}^{(s)} = \arctan \left(-\frac{(R_i^T g_n^s R_i)_{1,3}}{(R_i^T g_n^s R_i)_{2,3}} \right), \quad s = 1, \dots, n - 1. \quad (24)$$

4. Previous work

The method of angular reconstitution [4, 18] recovers the orientations corresponding to a given set of projection-images in a sequential manner. Specifically, it first determines the common lines between arbitrary three images. This establishes a coordinate system, and the orientations of all remaining projection-images are then recovered one after the other by using the common lines between any given image and those three images. However, due to the sequential nature of angular reconstitution, the method critically depends on correctly detecting the common lines between the first three images. As a result, when the input projection-images are noisy, this positioning might be wrong, which would lead to errors when inferring the relative orientations of the remaining central planes.

In [13], a non-sequential common-lines-based method was suggested, which estimates simultaneously the orientations of all projection-images. As such, contrary to the method of angular reconstitution, it does not suffer from accumulation of errors and is therefore robust even when the input images are noisy. However, this method may not be applied to projection-images of a molecule with C_n symmetry, since there is no way to guarantee a consistent choice of common lines, and so for each pair of images \hat{P}_{R_i} and \hat{P}_{R_j} we can only estimate $R_i^T g_n^{s_{ij}} R_j$ for an unknown s_{ij} , whereas to

apply the method in [13] all s_{ij} must be the same. Unfortunately, such a consistency in all s_{ij} cannot be guaranteed using the method of [13].

In [2], a method which successfully handles molecules with C_2 symmetry was proposed. The method is based on determining for every two images \hat{P}_{R_i} and \hat{P}_{R_j} both of their two common lines. Unfortunately, generalizations of this method to C_n for $n > 2$ are of little practical use, as it requires to detect all n common lines (Lemma 2.1) of every two images, which is impractical when the input images are noisy. Nevertheless, the method presented in the current paper is in some sense an extension of [2], but with two key differences. First, detecting all common lines between each pair of images is replaced by a maximum-likelihood-type procedure that directly estimates their relative orientation, from which their common lines can be easily computed. Second, our method takes advantage of self common lines, which do not exist in the case of C_2 symmetry.

5. Outline of our method

In this section, we provide an outline of our method for recovering the orientations of a given set of projection-images of a molecule with C_n symmetry with $n > 2$. Figure 3 depicts a flowchart of the method.

In what follows, we denote by v_i^T the third row of R_i , $i = 1, \dots, m$. Given projection-images P_1, \dots, P_m with corresponding unknown rotations R_1, \dots, R_m (to be estimated), the first step of our method, denoted as “relative viewing directions estimation” (Section 6), consists of estimating for each pair of projection-images P_i and P_j , $i \leq j$, one of the two 3×3 matrices $v_i v_j^T$ or $J v_i v_j^T J$, where $J = \text{diag}(-1, -1, 1)$, using common lines and self common lines of P_i and P_j . The two matrices $v_i v_j^T$ and $J v_i v_j^T J$ are indistinguishable using common lines due to the handedness ambiguity discussed in Section 1. We thus denote the estimated matrix by v_{ij} . The second step, which is denoted as “handedness synchronization” (Section 7), enforces that either all estimates v_{ij} have a spurious J , or none have at all. Once these estimates all correspond to a single hand, the next step, denoted as “viewing directions estimation”, consists of forming a $3m \times 3m$ symmetric matrix V whose (i, j) -th block of size 3×3 is given by v_{ij} . That is,

$$V_{ij} = \begin{cases} v_{ij}, & \text{if } i \leq j, \\ v_{ji}^T, & \text{if } i > j. \end{cases} \quad (25)$$

Depending on the output of the handedness synchronization step described above, the factorization

$$V = vv^T, \quad v \in \mathbb{R}^{3m}, \quad (26)$$

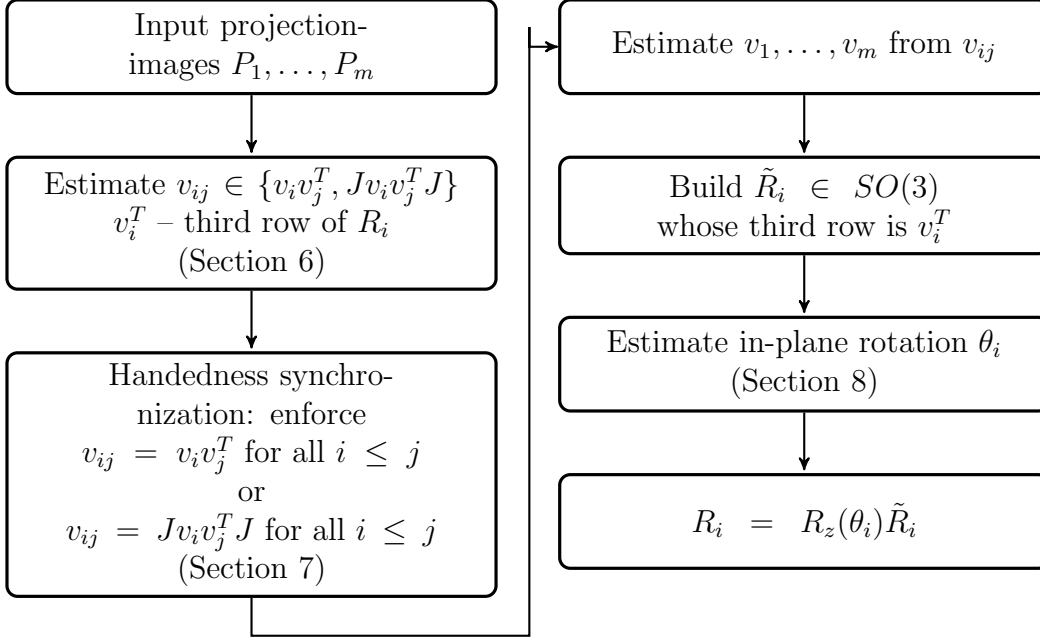


Figure 3: A flowchart illustrating the steps for estimating the orientations of projection-images of molecules with C_n symmetry.

yields at once either the estimates of the third rows v_i^T of all rotation matrices R_i , or the estimates of all J -multiplied third rows $v_i^T J$. The next step is to form m rotation matrices $\tilde{R}_1, \dots, \tilde{R}_m$ where the third row of each \tilde{R}_i is set to be equal to the estimate for either v_i^T or $v_i^T J$. The first two rows of each \tilde{R}_i are set arbitrarily (so that $\tilde{R}_i \in SO(3)$). In Lemma 8.1 below, we prove that for any $i \in [m]$ there exist $\theta_i \in [0, 2\pi/n)$ and $s_i \in [n]$ such that

$$g_n^{s_i} R_i = R_z(\theta_i) \tilde{R}_i, \quad (27)$$

where $R_z(\theta_i)$ is a rotation matrix that rotates vectors by an angle of θ_i about the z -axis (see (15)). As a result, since each R_i may be replaced by either $g_n^{s_i} R_i$ or $g_n^{s_i} R_i J$ for some $s_i \in [n-1]$, it suffices to recover the in-plane rotation angles $\theta_i \in [0, 2\pi/n)$. The step which consists of recovering all these angles θ_i is denoted by “in-plane rotation angles estimation” (Section 8). Finally, the last step is “orientations estimation” in which all rotation matrices $g_n^{s_i} R_i$ (or $g_n^{s_i} R_i J$) are formed using (27).

We next present a method for estimating the set of all relative viewing directions $\{v_i v_j^T \mid i \leq j, i, j = 1, \dots, m\}$ which may be applied to molecules with C_n symmetry with $n > 2$ (a full treatment of C_2 symmetry may be found in [2]). In addition, we

describe in Appendix A an alternative method that is applicable only to molecules with either C_3 or C_4 symmetry. While the method of Section 6 may be applied to molecules with C_3 or C_4 symmetry, the alternative method of Appendix A utilizes the underlying geometry that is induced by such molecules. As a result, it produces better results in practice and is much faster.

6. Relative viewing directions estimation for C_n symmetry with $n > 2$

Loosely speaking, estimating $\{v_i v_j^T \mid i, j = 1, \dots, m, i \leq j\}$ is based on inspecting for each pair of images all possible pairs of rotation matrices (discretized in some proper manner, as explained later on in Section 9), and finding the pair that induces common lines and self common lines which are most correlated. Such an approach is advantageous for the following two reasons:

1. By Lemma 2.1, any two images have n pairs of common lines, and by Corollary 3.2, any image has $\lfloor \frac{n-1}{2} \rfloor$ pairs of (non collinear) self common lines. Therefore, for any two images, the degree by which a given pair of candidate rotation matrices induces the correct relative orientation of the two images, may be ascertained with greater confidence as n increases. Specifically, if most of the common lines and self common lines that are induced by a given pair of candidate rotation matrices are highly correlated, then it is likely that these candidates correspond to the true rotation matrices.
2. Recall that any R_i may be replaced by $g_n^{s_i} R_i$ where $s_i \in [n-1]$ is arbitrary. In light of that, for each $i \in [m]$, if we write the third column $R_i^{(3)}$ of R_i in its spherical coordinates representation, i.e., $R_i^{(3)} = (\sin \theta_i \cos \phi_i, \sin \theta_i \sin \phi_i, \cos \theta_i)^T$ for some $\phi_i \in [0, 2\pi)$ and $\theta_i \in [0, \pi)$, then by a direct calculation, we get that for any $s_i \in [n]$,

$$g_n^{s_i} R_i^{(3)} = \left(\sin \theta_i \cos \left(\phi_i + \frac{2\pi s_i}{n} \right), \sin \theta_i \sin \left(\phi_i + \frac{2\pi s_i}{n} \right), \cos \theta_i \right)^T. \quad (28)$$

Thus, since for any ϕ_i there exists $s_i \in [n]$ such that $\phi_i + \frac{2\pi s_i}{n} \bmod 2\pi \in [0, 2\pi/n)$, it follows that instead of considering the set of “all possible” candidate rotations for each image, it suffices to only consider the set $SO_n(3)$ given by

$$SO_n(3) = \left\{ R \in SO(3) \mid \Phi(R^{(3)}) \in [0, 2\pi/n) \right\}, \quad (29)$$

where $\Phi: \mathbb{R}^3 \rightarrow [0, 2\pi)$ is the mapping $(\sin \theta \cos \phi, \sin \theta \sin \phi, \cos \theta)^T \mapsto \phi$ of any vector in \mathbb{R}^3 to its azimuthal angle in its spherical coordinates representation. For large n this significantly restricts the search space of the candidate rotation matrices.

In light of reason (2) above, throughout the remaining of this section, we assume without loss of generality that $R_1, \dots, R_m \in SO_n(3)$ (see (29)). The following lemma, whose proof is given in Appendix B.2, and the corollary that follows will be used in the sequel.

Lemma 6.1. *For any $n \in \mathbb{N}$, $n > 1$, and $l \in \mathbb{Z}$ such that $(l \bmod n) \neq 0$,*

$$\frac{1}{n} \sum_{s=0}^{n-1} g_n^{ls} = \text{diag}(0, 0, 1). \quad (30)$$

Corollary 6.2. *By applying (30) to any $n \in \mathbb{N}$, $n > 1$, with $l = 1$, we get that for any $i, j \in [m]$,*

$$\frac{1}{n} \sum_{s=0}^{n-1} R_i^T g_n^s R_j = R_i^T \left(\frac{1}{n} \sum_{s=0}^{n-1} g_n^s \right) R_j = R_i^T \text{diag}(0, 0, 1) R_j = v_i v_j^T. \quad (31)$$

At first glance, it would appear that the rotation matrices $R_1, \dots, R_m \in SO_n(3)$ may be estimated by searching for each pair of images for the pair of rotation matrices that induce pairs of lines whose values are most correlated. That is, since the values along common lines and self common lines have perfect correlation over all other pairs of lines, it follows from (10) and (22) that the pair of rotation matrices (R_i, R_j) attains the maximal value of $S_{\hat{P}_{R_i}, \hat{P}_{R_j}}: SO_n(3) \times SO_n(3) \rightarrow \mathbb{R}$, given by

$$\begin{aligned} S_{\hat{P}_{R_i}, \hat{P}_{R_j}}(\tilde{R}_i, \tilde{R}_j) &= \prod_{s=0}^{n-1} \text{Re} \int_{\xi} \hat{P}_{R_i}(\xi \cos \tilde{\alpha}_{ij}^{(s)}, \xi \sin \tilde{\alpha}_{ij}^{(s)}) \overline{\hat{P}_{R_j}(\xi \cos \tilde{\alpha}_{ji}^{(s)}, \xi \sin \tilde{\alpha}_{ji}^{(s)})} d\xi \\ &\prod_{k \in \{i, j\}} \prod_{s=1}^{\lfloor \frac{n-1}{2} \rfloor} \text{Re} \int_{\xi} \hat{P}_{R_k}(\xi \cos \tilde{\alpha}_{kk}^{(s)}, \xi \sin \tilde{\alpha}_{kk}^{(s)}) \hat{P}_{R_k}(\xi \cos \tilde{\alpha}_{kk}^{(n-s)}, \xi \sin \tilde{\alpha}_{kk}^{(n-s)}) d\xi, \end{aligned} \quad (32)$$

with $\text{Re}(z)$ denoting the real part of $z \in \mathbb{C}$, where each ray in each of the images in (32) is normalized to have norm equal to one, and where (in accordance with (16)

and (24)),

$$\begin{aligned}\tilde{\alpha}_{ij}^{(s)} &= \arctan \left(-\frac{\left(\tilde{R}_i^T g_n^s \tilde{R}_j\right)_{1,3}}{\left(\tilde{R}_i^T g_n^s \tilde{R}_j\right)_{2,3}} \right), & \tilde{\alpha}_{ji}^{(s)} &= \arctan \left(-\frac{\left(\tilde{R}_i^T g_n^s \tilde{R}_j\right)_{3,1}}{\left(\tilde{R}_i^T g_n^s \tilde{R}_j\right)_{3,2}} \right), & s &= 0, \dots, n-1, \\ \tilde{\alpha}_{kk}^{(s)} &= \arctan \left(-\frac{\left(\tilde{R}_k g_n^s \tilde{R}_k\right)_{1,3}}{\left(\tilde{R}_k g_n^s \tilde{R}_k\right)_{2,3}} \right), & k \in \{i, j\}, & s &= 1, \dots, \left\lfloor \frac{n-1}{2} \right\rfloor.\end{aligned}\tag{33}$$

However, for any $i < j \in [m]$, the maximum of (32) over $SO_n(3) \times SO_n(3)$ is not necessarily unique, and—depending on R_i and R_j —might be attained by other pairs of rotation matrices besides (R_i, R_j) . For example, by (33), any pair of rotation matrices (R_i^*, R_j^*) such that

$$\left\{ R_i^{*T} g_n^s R_i^* \right\}_{s=1}^{n-1} = \left\{ R_i^T g_n^s R_i \right\}_{s=1}^{n-1}, \quad \left\{ R_j^{*T} g_n^s R_j^* \right\}_{s=1}^{n-1} = \left\{ R_j^T g_n^s R_j \right\}_{s=1}^{n-1}, \tag{34}$$

and

$$\left\{ R_i^{*T} g_n^s R_j^* \right\}_{s=0}^{n-1} = \left\{ R_i^T g_n^s R_j \right\}_{s=0}^{n-1}, \tag{35}$$

would also maximize (32). Nevertheless, while not every maximizer (R_i^*, R_j^*) of (32) is necessarily equal to (R_i, R_j) , we observed empirically (using extensive simulations) that all such maximizers (R_i^*, R_j^*) satisfy (34) and (35). As a result, it follows from (31) that

$$\frac{1}{n} \sum_{s=0}^{n-1} R_i^{*T} g_n^s R_j^* = \frac{1}{n} \sum_{s=0}^{n-1} R_i^T g_n^s R_j = v_i v_j^T, \tag{36}$$

where v_i^T and v_j^T are the third rows of R_i and R_j , respectively. That is, any outer product $v_i v_j^T$ is invariant to permutations of the n common lines in \hat{P}_{R_i} and \hat{P}_{R_j} . Thus, for any $i < j \in [m]$, we choose an arbitrary pair (R_i^*, R_j^*) which maximizes (32), and obtain an estimate v_{ij} for $v_i v_j^T$ which, due to the inherent handedness ambiguity satisfies $v_{ij} \in \{v_i v_j^T, J v_i v_j^T J\}$. In a similar vein, it follows from (34) and (31) that,

for any $i \in [m]$, any maximizer (R_i^*, R_j^*) of (32) yields

$$\frac{1}{n} \sum_{s=0}^{n-1} R_i^{*T} g_n^s R_i^* = \frac{1}{n} \sum_{s=0}^{n-1} R_i^T g_n^s R_i = v_i v_i^T. \quad (37)$$

Thus, for any $i \in [m]$, any of the $m-1$ pairs (R_i^*, R_j^*) where $j \neq i$, induces an estimate v_{ii}^j for $v_i v_i^T$ using (37). In practice, however, due to self common lines misidentification, any such estimate v_{ii}^j of $v_i v_i^T$ may contain some error. Thus, choosing any one of the estimates v_{ii}^j to be the single estimate v_{ii} for $v_i v_i^T$ is sub-optimal. Furthermore, averaging over all $m-1$ estimates v_{ii}^j doesn't make any sense, since due to the handedness ambiguity, $v_{ii}^j \in \{v_i v_i^T, J v_i v_i^T J\}$ independently of other estimates. Instead, since any $v_i v_i^T$ is a matrix of rank-1, we set v_{ii} to be equal to the estimate v_{ii}^j that is closest to a rank-1 matrix. Specifically, for every $i \in [m]$ we compute the estimates v_{ii}^j , $j \neq i$, and for every such estimate we find (using SVD) its three singular-values $s_{i,1}^{(j)}, s_{i,2}^{(j)}, s_{i,3}^{(j)} \in \mathbb{R}$, and set $v_{ii} = v_{ii}^{j^*}$ where

$$j^* \leftarrow \arg \min_{\substack{j=1, \dots, m \\ j \neq i}} \left\| \left(s_{i,1}^{(j)}, s_{i,2}^{(j)}, s_{i,3}^{(j)} \right)^T - (1, 0, 0)^T \right\|_2. \quad (38)$$

The procedure for finding all estimates v_{ij} and v_{ii} which, due to the inherent handedness ambiguity, satisfy $v_{ij} \in \{v_i v_j^T, J v_i v_j^T J\}$ and $v_{ii} \in \{v_i v_i^T, J v_i v_i^T J\}$ is summarized in Algorithm 1.

7. Handedness synchronization

At this stage, we have determined the estimates v_{ij} , $i \leq j \in [m]$, of all relative viewing directions, where for each estimate v_{ij} either $v_{ij} = v_i v_j^T$ or $v_{ij} = J v_i v_j^T J$ independently of other estimates. In this section, we describe the ‘‘handedness synchronization’’ step, where the task is to manipulate these estimates v_{ij} so that either $v_{ij} = v_i v_j^T$ for all $i \leq j \in [m]$, or $v_{ij} = J v_i v_j^T J$ for all $i \leq j \in [m]$. Once this procedure is completed, we can form the matrix V from (25) and infer the third rows v_i^T of all rotation matrices R_i (or all J -multiplied third rows $v_i^T J$) using (26). Handedness synchronization is done in two steps. The first step synchronizes the estimates v_{ij} , $i < j \in [m]$. The second step synchronizes each of the remaining estimates v_{ii} , $i \in [m]$, with the synchronized estimates from the first step. The reason for separating the synchronization of v_{ij} from that of v_{ii} will be clarified below.

Algorithm 1 Estimate v_{ij} , $i \leq j \in [m]$, for molecules with C_n symmetry, with $n > 2$

- 1: **Input:** (i) Images \hat{P}_{R_i} , $i \in [m]$. (ii) Cyclic symmetry order $n > 2$.
 - 2: **for** $i < j \in [m]$ **do**
 - 3: $\left(R_i^*, R_j^*\right) \leftarrow \underset{\tilde{R}_i, \tilde{R}_j \in SO_n(3)}{\operatorname{argmax}} S_{\hat{P}_{R_i}, \hat{P}_{R_j}}\left(\tilde{R}_i, \tilde{R}_j\right)$ ▷ (32)
 - 4: $v_{ij} \leftarrow \frac{1}{n} \sum_{s=0}^{n-1} R_i^{*T} g_n^s R_j^*$ ▷ (36)
 - 5: $v_{ii}^j \leftarrow \frac{1}{n} \sum_{s=0}^{n-1} R_i^{*T} g_n^s R_i^*$ ▷ (37)
 - 6: $v_{jj}^i \leftarrow \frac{1}{n} \sum_{s=0}^{n-1} R_j^{*T} g_n^s R_j^*$ ▷ (37)
 - 7: **end for**
 - 8: **for** $i \in [m]$ **do**
 - 9: $s_{i,1}^{(j)}, s_{i,2}^{(j)}, s_{i,3}^{(j)} \leftarrow \text{singular-values}\left(v_{ii}^j\right)$, $j = 1, \dots, m$, $j \neq i$ ▷ using SVD
 - 10: $j^* \leftarrow \underset{j \neq i}{\operatorname{arg min}}_{j=1, \dots, m} \left\| \left(s_{i,1}^{(j)}, s_{i,2}^{(j)}, s_{i,3}^{(j)}\right)^T - (1, 0, 0)^T \right\|_2$ ▷ (38)
 - 11: $v_{ii} \leftarrow v_{ii}^{j^*}$
 - 12: **end for**
 - 13: **Output:** v_{ij} , $i \leq j \in [m]$. ▷ $v_{ij} \in \{v_i v_j^T, J v_i v_j^T J\}$
-

7.1. Step 1: Synchronizing the estimates v_{ij} , $i < j \in [m]$

We employ a procedure similar to the one described in [13]. Specifically, the task of synchronizing the set of estimates $\{v_{ij} \mid i < j \in [m]\}$ may be reduced to the task of partitioning this set into the following two disjoint sets

$$S_1 = \left\{v_{ij} \mid v_{ij} = v_i v_j^T\right\}, \quad S_2 = \left\{v_{ij} \mid v_{ij} = J v_i v_j^T J\right\}. \quad (39)$$

Indeed, once all estimates v_{ij} are partitioned into S_1 and S_2 , we can choose either one of the sets (does not matter which one), and replace each estimate v_{ij} in it by $J v_{ij} J$. As a result, since $J^2 = I$, we get that either $v_{ij} = v_i v_j^T$ for all $i < j \in [m]$, or $v_{ij} = J v_i v_j^T J$ for all $i < j \in [m]$, as needed. We now describe how we obtain such a partition (39).

Let us define the ‘‘handedness graph’’ $\Gamma = (V, E)$ to be the undirected graph whose set of nodes V consists of all estimates v_{ij} , $i < j \in [m]$, that is

$$V = \left\{v_{ij} \mid i < j, i, j = 1, \dots, m\right\}, \quad (40)$$

and whose set of edges E consists of the undirected edges between all triplets of

estimates v_{ij} , v_{jk} , and v_{ik} (hence each triplet forms a “triangle”), that is,

$$E = \bigcup_{i < j < k \in [m]} \left\{ (v_{ij}, v_{jk}), (v_{jk}, v_{ik}), (v_{ik}, v_{ij}) \right\}. \quad (41)$$

The weight of each edge is set to either $+1$ or -1 as explained below. For each $i < j < k \in [m]$, we consider the three estimates v_{ij} , v_{jk} and v_{ik} , along with the “triangle” they form in the graph. The goal is to set the weight $+1$ to all edges of the triangle whose incident nodes correspond to estimates that belong to the same set in (39), and to set the weight of all other edges to -1 . A crucial observation is that for any $i < j < k \in [m]$,

$$v_i v_j^T v_j v_k^T = v_i v_k^T. \quad (42)$$

As such, we check which of the following expressions

$$\begin{array}{ll} 1. v_{ij} v_{jk} - v_{ik} & 3. v_{ij} \mathbf{J} v_{jk} \mathbf{J} - v_{ik} \\ 2. \mathbf{J} v_{ij} \mathbf{J} v_{jk} - v_{ik} & 4. v_{ij} v_{jk} - \mathbf{J} v_{ik} \mathbf{J} \end{array} \quad (43)$$

equals the 3×3 zero matrix, and assign the weight of each of the three edges in the corresponding triangle as illustrated in Figure 4. The expressions listed in (43) allow to decide for each triplet v_{ij} , v_{jk} , v_{ik} which nodes belong to the same set in (39) and which belong to different sets. For three nodes the only two possibilities are that either all nodes belong to the same set (case 1 in (43)), or that one node belongs to one of the sets and the remaining two nodes belong to the other set (cases 2, 3, 4 in (43)). Thus, by (43) we determine the partition (39) “locally” for each triplet of nodes. For example, if all three estimates belong to the same set in (39) (i.e., either all belong to S_1 , or all belong to S_2), then the first expression in (43) is equal to the zero matrix, meaning that the weights of all three edges in the corresponding triangle in the graph are set to $+1$ (as per Figure 4a). Indeed, in case v_{ij} , v_{jk} , and v_{ik} belong to S_1 , then since $v_j^T v_j = 1$, we get

$$v_{ij} v_{jk} - v_{ik} = v_i v_j^T v_j v_k^T - v_i v_k^T = 0,$$

and in case all these three estimates belong to S_2 , then since $J^2 = I$, it also follows that

$$v_{ij} v_{jk} - v_{ik} = J v_i v_j^T J J v_j v_k^T J - J v_i v_k^T J = 0.$$

Once we have determined the local assignment of each triplet of nodes (via the weights on the edges between the vertices corresponding to the nodes), we obtain a global partition into the sets in (39) similarly to [13]. Specifically, we define the

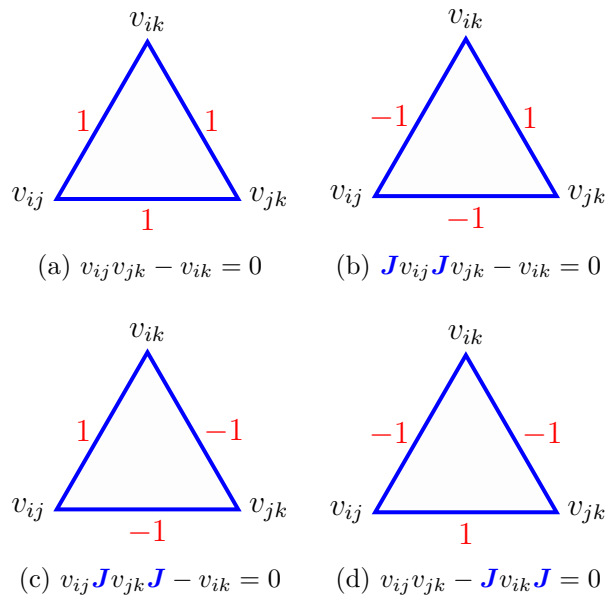


Figure 4: Subgraphs (triangles) of the handedness graph Γ corresponding to the four configurations in (43). The edges have weight equal to +1 if the incident nodes belong to the same set in (39), and equal to -1 otherwise.

weighted adjacency matrix of Γ , also denoted by Γ , as the $\binom{m}{2} \times \binom{m}{2}$ matrix whose entries are given by

$$\Gamma_{(i,j),(k,l)} = \begin{cases} 1, & \text{if } |\{i,j\} \cap \{k,l\}| = 1, \text{ and } v_{ij}, v_{kl} \text{ are in the same set of (39),} \\ -1, & \text{if } |\{i,j\} \cap \{k,l\}| = 1, \text{ and } v_{ij}, v_{kl} \text{ are in different sets of (39),} \\ 0, & \text{if } |\{i,j\} \cap \{k,l\}| = 0. \end{cases} \quad (44)$$

We then calculate the eigenvector u_Γ that corresponds to the leading eigenvalue of the matrix Γ . As was shown in [13], this eigenvalue has multiplicity one and its corresponding eigenvector $u_\Gamma \in \{-1, 1\}^{\binom{m}{2}}$ encodes the set membership of the estimates. Specifically, if $u_\Gamma(i, j) = 1$ then v_{ij} belongs to one of the sets of (39), and if $u_\Gamma(i, j) = -1$ then v_{ij} belongs to the other set of (39). As such, by J -conjugating all estimates in either one of the sets we are guaranteed that either $v_{ij} = v_i v_j^T$ for all $i < j \in [m]$, or $v_{ij} = J v_i v_j^T J$ for all $i < j \in [m]$.

Notice that, in practice, the estimates v_{ij} are computed from noisy projection-images, and thus for many triplets of estimates none of the four expressions listed in (43) might be equal exactly to the zero matrix. Thus, instead, we search for the expression that is as close as possible to the zero matrix. Specifically, we minimize

$$P_{ijk}(\mu_{ij}, \mu_{jk}) = \|J^{\mu_{ij}} v_{ij} J^{\mu_{ij}} \cdot J^{\mu_{jk}} v_{jk} J^{\mu_{jk}} - J^{\mu_{ik}} v_{ik} J^{\mu_{ik}}\|_F \quad (45)$$

over $\mu_{ij}, \mu_{jk}, \mu_{ik} \in \{0, 1\}$, subject to the constraint that $\mu_{ij} + \mu_{jk} + \mu_{ik} \leq 1$, where each possible triplet $(\mu_{ij}, \mu_{jk}, \mu_{ik}) \in \{0, 1\}^3$ corresponds to one of the four expressions in (43), and $\|\cdot\|_F$ denotes the Frobenius norm.

7.2. Step 2: Synchronizing the estimates v_{ii} , $i \in [m]$

The second step of handedness synchronization consists of synchronizing each of the estimates v_{ii} so that if the previous step (described in Section 7.1) resulted in every v_{ij} satisfying $v_{ij} = v_i v_j^T$, then the goal is to enforce that $v_{ii} = v_i v_i^T$ for every $i \in [m]$. Otherwise, if the output of the previous step is such that every v_{ij} satisfies $v_{ij} = J v_i v_j^T J$, then the goal is to enforce that $v_{ii} = J v_i v_i^T J$ for every $i \in [m]$. Recall, however, that it is unknown which of the above two possible outputs was obtained. Nevertheless, since $v_i^T v_i = 1$ for any $i \in [m]$, and since $J^2 = I$, it follows that for any $j \in [m]$,

$$(v_i v_i^T)(v_j v_j^T) = v_i v_j^T, \quad (46)$$

$$(J v_i v_i^T J)(J v_j v_j^T J) = J v_i v_j^T J. \quad (47)$$

As such, we can in principle synchronize every v_{ii} by choosing an arbitrary v_{ij} such that $j \neq i$, and reset v_{ii} as follows:

$$v_{ii} \leftarrow \begin{cases} v_{ii}, & \text{if } v_{ii}v_{ij} = v_{ij}, \\ Jv_{ii}J, & \text{if } Jv_{ii}Jv_{ij} = v_{ij}. \end{cases} \quad (48a)$$

$$v_{ii} \leftarrow \begin{cases} v_{ii}, & \text{if } v_{ii}v_{ij} = v_{ij}, \\ Jv_{ii}J, & \text{if } Jv_{ii}Jv_{ij} = v_{ij}. \end{cases} \quad (48b)$$

Indeed, if $v_{ij} = v_i v_j^T$ (which we cannot tell), then by (46), case (48a) occurs if $v_{ii} = v_i v_i^T$ and therefore v_{ii} should not be altered. Similarly, if $v_{ij} = v_i v_j^T$ then by (46), case (48b) occurs if $v_{ii} = Jv_i v_i^T J$ (since $J^2 = I$) so that by assigning $v_{ii} \leftarrow Jv_{ii}J$ we indeed end up having $v_{ii} = v_i v_i^T$, as needed. The case of $v_{ij} = Jv_i v_j^T J$ is analogous in light of (47).

In practice, however, since each of the above estimates is computed from noisy images, it might be that neither (48a) nor (48b) hold. In addition, it is desirable to synchronize each v_{ii} based on all estimates v_{ij} such that $j > i$ rather than only using a single such estimate. Thus, instead, each estimate v_{ii} is set according to the majority-vote over all v_{ij} . Specifically, let us denote by $\text{sign}(x)$ the sign function (which equals 1 if $x \geq 0$ and equals -1 otherwise). Then, for every $i \in [m]$ we reset v_{ii} to be $Jv_{ii}J$ in case that

$$\sum_{\substack{j \in [m] \\ j > i}} \text{sign}(\|Jv_{ii}Jv_{ij} - v_{ij}\|_F - \|v_{ii}v_{ij} - v_{ij}\|_F) < 0. \quad (49)$$

Once this second step is completed, we are guaranteed that all estimates are synchronized, i.e., either $v_{ij} = v_i v_j^T$ for all $i \leq j \in [m]$, or $v_{ij} = Jv_i v_j^T J$ for all $i \leq j \in [m]$. As such, we then construct the matrix V of (25), factorize it as in (26), and obtain all third rows v_1^T, \dots, v_m^T (or $v_1^T J, \dots, v_m^T J$). The procedure for handedness synchronization is summarized in Algorithm 2.

Note that synchronizing the estimates v_{ij} , $i < j \in [m]$, is done separately from synchronizing the estimates v_{ii} . Synchronizing v_{ij} based on (42) involves triplets of indices $i < j < k$, and so is the construction of the graph Γ in (44). On the other hand, the synchronization of v_{ii} is based on pairs of indices (see (48a) and (48b)). So while it may be better to synchronize v_{ij} and v_{ii} simultaneously, it is currently unclear how to combine the pairwise information required for synchronizing v_{ii} into the triplets structure required for constructing Γ .

8. In-plane rotation angles estimation

At this stage, all third rows v_1^T, \dots, v_m^T (or $v_1^T J, \dots, v_m^T J$) of the rotation matrices R_1, \dots, R_m (or $R_1 J, \dots, R_m J$) have been obtained. In this section, we describe a

Algorithm 2 Handedness synchronization of the relative viewing directions estimates

- 1: **Input:** Relative viewing directions estimates v_{ij} , $i \leq j \in [m]$ (computed by Algorithm 1).
 - 2: **Initialization:** Matrix Γ of size $\binom{m}{2} \times \binom{m}{2}$ with all entries set to zero.
 - 3: **for** $i < j < k \in [m]$ **do** ▷ Section 7.1
 - 4: $(\mu_{ij}^*, \mu_{jk}^*, \mu_{ik}^*) \leftarrow \underset{\substack{\mu_{ij}, \mu_{jk}, \mu_{ik} \in \{0,1\} \\ \mu_{ij} + \mu_{jk} + \mu_{ik} \leq 1}}{\operatorname{argmin}} P_{ijk}(\mu_{ij}, \mu_{jk}, \mu_{ik})$ ▷ (45)
 - 5: $\Gamma_{(j,k),(i,j)}, \Gamma_{(i,j),(j,k)} \leftarrow (-1)^{(\mu_{ij}^* - \mu_{jk}^*)}$ ▷ Γ is an undirected graph (see (44))
 - 6: $\Gamma_{(k,i),(j,k)}, \Gamma_{(j,k),(k,i)} \leftarrow (-1)^{(\mu_{jk}^* - \mu_{ik}^*)}$
 - 7: $\Gamma_{(i,j),(k,i)}, \Gamma_{(k,i),(i,j)} \leftarrow (-1)^{(\mu_{ik}^* - \mu_{ij}^*)}$
 - 8: **end for**
 - 9: $u_\Gamma \leftarrow \underset{\|v\|=1}{\operatorname{argmax}} v^T \Gamma v$ ▷ u_Γ is the eigenvector of the leading eigenvalue of Γ
 - 10: **for** $i < j \in [m]$ **do**
 - 11: **if** $u_\Gamma(i, j) < 0$ **then**
 - 12: $v_{ij} \leftarrow Jv_{ij}J$
 - 13: **end if**
 - 14: **end for**
 - 15: **for** $i \in [m]$ **do** ▷ Section 7.2
 - 16: **if** $\sum_{\substack{j \in [m] \\ j > i}} \operatorname{sign}(\|Jv_{ii}Jv_{ij} - v_{ij}\|_F - \|v_{ii}v_{ij} - v_{ij}\|_F) < 0$ **then**
 - 17: $v_{ii} \leftarrow Jv_{ii}J$
 - 18: **end if**
 - 19: **end for**
 - 20: **Output:** v_{ij} , $i \leq j \in [m]$.
-

procedure to determine the remaining first two rows in each of these rotation matrices. The following lemma shows that any two such rows are determined by a single parameter, namely an in-plane rotation angle about the z -axis (the axis of symmetry).

Lemma 8.1. *Let R and \tilde{R} be any two rotation matrices with identical third rows. Then, for any $n \in \mathbb{N}$, there exist a unique $\theta \in [0, 2\pi/n)$ and a unique $s \in [n]$ such that*

$$g_n^s R = R_z(\theta) \tilde{R}, \quad (50)$$

where $R_z(\theta)$ (given by (15)) is the matrix that rotates vectors by an angle θ about the z -axis.

The proof of Lemma 8.1 is given in Appendix B.3. In light of Lemma 8.1, we next form m rotation matrices $\tilde{R}_1, \dots, \tilde{R}_m$ by setting the third row of each \tilde{R}_i to be equal to the estimate of the third row of R_i (see Section 7), and by arbitrarily setting the first two rows of each \tilde{R}_i (while ensuring that $\tilde{R}_i \in SO(3)$). As a result, due to Lemma 8.1, for any $i \in [m]$, there only remains to recover the in-plane rotation angle $\theta_i \in [0, 2\pi/n)$, and form the matrix $R_z(\theta_i) \tilde{R}_i$. In principle, all such angles θ_i may be determined in a sequential manner. However, we instead employ a more robust approach in which all θ_i are determined in a single step. Specifically, as we next show, the task of determining all angles $\theta_i \in [0, 2\pi/n)$ may be reduced to finding for every (i, j) , $i \leq j \in [m]$, the relative in-plane rotation angles

$$\theta_{ij} := -\theta_i + \theta_j \pmod{2\pi/n}. \quad (51)$$

Indeed, by the definition of θ_{ij} , there exist unique $k_{ij} \in \{0, 1\}$, $i \leq j \in [m]$, such that

$$\theta_{ij} = -\theta_i + \theta_j + \frac{2\pi k_{ij}}{n} \in [0, 2\pi/n). \quad (52)$$

Thus, by letting Q be the $m \times m$ matrix whose (i, j) -th entry Q_{ij} is equal to $e^{m\theta_{ij}}$, it follows that

$$Q_{ij} = e^{m\theta_{ij}} = e^{i(n(-\theta_i + \theta_j) + 2\pi k_{ij})} = e^{m(-\theta_i + \theta_j)}, \quad i \leq j = 1, \dots, m. \quad (53)$$

As such, Q is a hermitian rank-1 matrix whose factorization is given by

$$Q = qq^H, \quad q = \left(e^{m\theta_1}, \dots, e^{m\theta_m} \right)^H, \quad (54)$$

from which all angles $\theta_i \in [0, 2\pi/n)$ may be retrieved using

$$\theta_i = \frac{1}{n} \arccos\left(\frac{q_i + \bar{q}_i}{2}\right). \quad (55)$$

Since Q is a rank-1 matrix, its factorization (54) yields the eigenvector αq where $\alpha \in \mathbb{C}$ with $|\alpha| = 1$ is arbitrary and unknown. As a result, (55) actually yields the angles $\theta + \theta_i$, $i \in [m]$, for some arbitrary, unknown $\theta \in [0, 2\pi)$. This poses no problem, since for any $\theta \in \mathbb{R}$, recovering $R_z(\theta + \theta_i)\tilde{R}_i = R_z(\theta)R_z(\theta_i)\tilde{R}_i$ is just as good, as we have the degree of freedom of applying any single in-plane rotation about the z -axis to all rotation matrices (see the paragraph following (4)). In light of (52)–(55), we describe below how to determine all θ_{ij} of (51). We then form the matrix Q above, obtain its factorization (54) using SVD, and recover all in-plane rotation angles θ_i using (55).

By applying Lemma 8.1 to any two rotation matrices R_i and R_j , we get that there exist $s_i, s_j \in [n]$ and unique angles $\theta_i, \theta_j \in [0, 2\pi/n)$, such that for any $s \in [n]$,

$$R_i^T g_n^s R_j = \left(g_n^{-s_i} R_z(\theta_i) \tilde{R}_i\right)^T g_n^s \left(g_n^{-s_j} R_z(\theta_j) \tilde{R}_j\right) = \tilde{R}_i^T R_z\left(-\theta_i + \theta_j + \frac{2\pi s_{ij}}{n}\right) \tilde{R}_j, \quad (56)$$

where the last equality follows by denoting $s_{ij} = s_i + s - s_j$ and using the fact that $g_n^{s_{ij}} = R_z\left(\frac{2\pi s_{ij}}{n}\right)$. As such,

$$\begin{aligned} \left\{ R_i^T g_n^s R_j \right\}_{s \in [n]} &= \left\{ \tilde{R}_i^T R_z\left(-\theta_i + \theta_j + \frac{2\pi s}{n}\right) \tilde{R}_j \right\}_{s \in [n]} \\ &= \left\{ \tilde{R}_i^T R_z\left(\theta_{ij} + \frac{2\pi s}{n}\right) \tilde{R}_j \right\}_{s \in [n]}, \end{aligned} \quad (57)$$

where the second equality used (51) and the fact that $R_z(\phi) = R_z(\phi \bmod 2\pi)$ for any $\phi \in \mathbb{R}$. Given θ_i and θ_j , exactly one of the angles among $-\theta_i + \theta_j + \frac{2\pi s}{n}$, $s \in [n]$, lies in $[0, 2\pi/n)$. Thus, by (51) and (57), θ_{ij} is the only angle in $[0, 2\pi/n)$ which satisfies

$$\left\{ R_i^T g_n^s R_j \right\}_{s \in [n]} = \left\{ \tilde{R}_i^T R_z\left(\theta_{ij} + \frac{2\pi s}{n}\right) \tilde{R}_j \right\}_{s \in [n]}. \quad (58)$$

Equation (58) is the set of all possible relative orientations between \hat{P}_{R_i} and \hat{P}_{R_j} .

Thus, if we know θ_{ij} in (58), then the common lines between \hat{P}_{R_i} and \hat{P}_{R_j} induced by these relative orientations will perfectly correlate (see (10)). Therefore, for any $i < j \in [m]$, we set the angle θ_{ij} to be the maximizer over all $\theta \in [0, 2\pi/n)$ of

$$\Upsilon(\theta) = \prod_{s=0}^{n-1} \operatorname{Re} \int_{\xi} \hat{P}_{R_i} \left(\xi \cos \alpha_{ij}^{(\theta,s)}, \xi \sin \alpha_{ij}^{(\theta,s)} \right) \overline{\hat{P}_{R_j} \left(\xi \cos \alpha_{ji}^{(\theta,s)}, \xi \sin \alpha_{ji}^{(\theta,s)} \right)} d\xi, \quad (59)$$

where each ray in each image in (59) is normalized to have norm equal one, and where (in accordance with (16)), for any $s = 0, \dots, n-1$,

$$\begin{aligned} \alpha_{ij}^{(\theta,s)} &= \arctan \left(-\frac{\left(\tilde{R}_i^T R_z \left(\theta + \frac{2\pi s}{n} \right) \tilde{R}_j \right)_{1,3}}{\left(\tilde{R}_i^T R_z \left(\theta + \frac{2\pi s}{n} \right) \tilde{R}_j \right)_{2,3}} \right), \\ \alpha_{ji}^{(\theta,s)} &= \arctan \left(-\frac{\left(\tilde{R}_i^T R_z \left(\theta + \frac{2\pi s}{n} \right) \tilde{R}_j \right)_{3,1}}{\left(\tilde{R}_i^T R_z \left(\theta + \frac{2\pi s}{n} \right) \tilde{R}_j \right)_{3,2}} \right). \end{aligned} \quad (60)$$

As a result, any θ_{ij} of (51) may be obtained by optimizing Υ of (59) over all $\theta \in [0, 2\pi/n)$. The procedure for determining all in-plane rotation angles is summarized in Algorithm 3.

Based on Algorithms 1, 2, 3 and on Section 5, the end-to-end algorithm for recovering all rotation matrices R_1, \dots, R_m is summarized in Algorithm 4. Note that the fact that we assumed in (4) without loss of generality that the axis of symmetry coincides with the z -axis, means that any reconstructed volume that is based on the output rotation matrices of Algorithm 4 will have its axis of symmetry aligned with the z -axis as well.

9. Numerical experiments

We implemented Algorithm 4 in Matlab and tested it on both simulated and experimental projection-images. Section 9.1 provides some of the implementation details of Algorithm 4, and Section 9.2 analyzes its time and space complexity. Section 9.3 describes the experiments conducted using noisy simulated projection-images of the three-dimensional density map EMD-6458 [20], which has C_{11} symmetry. Section 9.4 presents results for the Trimeric HIV-1 envelope glycoprotein [22] which has C_3 symmetry. Section 9.5 focuses on the Human HCN1 hyperpolarization-activated

Algorithm 3 Recover the in-plane rotation angles

- 1: **Input:** (i) Images \hat{P}_{R_i} , $i = 1, \dots, m$. (ii) $\tilde{R}_i \in SO(3)$, $i \in [m]$, where the third row of \tilde{R}_i is equal to the estimate of the third row of R_i . (iii) Discretization parameter $K \in \mathbb{N}$ (iv) Cyclic symmetry order n .
 - 2: **Initialize:** (i) Array Υ of length K . (ii) Matrix Q of size $m \times m$ with all entries set to zero.
 - 3: **for** $i < j \in [m]$ **do**
 - 4: **for** $k \in [K]$ **do**
 - 5: $\theta_k \leftarrow \frac{2\pi}{nK}(k-1)$
 - 6: $R_{ij}(\theta_k, s) \leftarrow \tilde{R}_i^T R_z\left(\theta_k + \frac{2\pi s}{n}\right) \tilde{R}_j$, $s = 0, \dots, n-1$
 - 7: $\alpha_{ij}^{(\theta_k, s)} \leftarrow \arctan\left(-\frac{(R_{ij}(\theta_k, s))_{1,3}}{(R_{ij}(\theta_k, s))_{2,3}}\right)$, $s = 0, \dots, n-1$ \triangleright (60)
 - 8: $\alpha_{ji}^{(\theta_k, s)} \leftarrow \arctan\left(-\frac{(R_{ij}(\theta_k, s))_{3,1}}{(R_{ij}(\theta_k, s))_{3,2}}\right)$, $s = 0, \dots, n-1$ \triangleright (60)
 - 9: $\Upsilon(\theta_k) \leftarrow \prod_{s=0}^{n-1} \text{Re} \int_{\xi} \hat{P}_{R_i}\left(\xi \cos \alpha_{ij}^{(\theta_k, s)}, \xi \sin \alpha_{ij}^{(\theta_k, s)}\right) \overline{\hat{P}_{R_j}\left(\xi \cos \alpha_{ji}^{(\theta_k, s)}, \xi \sin \alpha_{ji}^{(\theta_k, s)}\right)} d\xi$
 $\triangleright \hat{P}_{R_i}$ and \hat{P}_{R_j} should be normalized (see (59))
 - 10: **end for**
 - 11: $k^* \leftarrow \arg \max_k \Upsilon(\theta_k)$
 - 12: $\theta_{ij} \leftarrow \frac{2\pi}{nK}(k^* - 1)$ $\triangleright \theta_{ij} = -\theta_i + \theta_j \pmod{2\pi/n}$
 - 13: $Q_{ij} \leftarrow e^{in\theta_{ij}}$, $Q_{ji} \leftarrow e^{-in\theta_{ij}}$ \triangleright (53)
 - 14: **end for**
 - 15: $Q \leftarrow Q + I$ \triangleright set $Q_{ii} = 1$ in accordance with (53) and (54)
 - 16: $q \leftarrow \underset{\|u\|=\sqrt{m}}{\text{argmax}} u^H Q u$ $\triangleright q$ is the eigenvector of the leading eigenvalue of Q (54)
 - 17: **for** $i \in [m]$ **do**
 - 18: $\theta_i \leftarrow \frac{1}{n} \arccos\left(\frac{q_i + \bar{q}_i}{2}\right)$ $\triangleright q_i = e^{-in\theta_i}$ (55)
 - 19: **end for**
 - 20: **Output:** θ_i , $i \in [m]$. $\triangleright R_z(\theta_i) \tilde{R} = g_n^{s_i} R_i$ for some $s_i \in [n]$
-

Algorithm 4 Orientations estimation for projection-images of molecules with C_n symmetry

- 1: **Input:** (i) Images \hat{P}_{R_i} , $i = 1, \dots, m$. (ii) Cyclic symmetry order $n \in \mathbb{N}$, $n > 2$.
 - 2: **Initialize:** A matrix V of size $3m \times 3m$.
 - 3: Find estimates $\{v_{ij}\}_{i < j=1}^m$ and $\{v_{ii}\}_{i=1}^m$ using Algorithm 1
 - 4: Synchronize the handedness of $\{v_{ij}\}_{i < j=1}^m$ and $\{v_{ii}\}_{i=1}^m$ using Algorithm 2
 - 5: **for** $i < j \in [m]$ **do**
 - 6: $V_{ij} \leftarrow v_{ij}$, $V_{ji} \leftarrow v_{ij}^T$, $V_{ii} \leftarrow v_{ii}$ \triangleright (25)
 - 7: **end for**
 - 8: $\tilde{v} \leftarrow \underset{\|u\|=1}{\operatorname{argmax}} u^T V u$ $\triangleright \mathbb{R}^{3m} \ni \tilde{v} = (\tilde{v}_1^T, \dots, \tilde{v}_m^T)^T$
 - 9: **for** $i \in [m]$ **do**
 - 10: Construct an arbitrary $\tilde{R}_i \in SO(3)$ whose third row is $\frac{\tilde{v}_i^T}{\|\tilde{v}_i\|}$
 - 11: **end for**
 - 12: Estimate the in-plane rotation angles $\{\theta_i\}_{i=1}^m$ using Algorithm 3
 - 13: **for** $i \in [m]$ **do**
 - 14: $R_i^* \leftarrow R_z(\theta_i) \tilde{R}_i$ \triangleright (27)
 - 15: **end for**
 - 16: **Output:** R_i^* , $i \in [m]$. $\triangleright \hat{P}_{R_i^*} = \hat{P}_{R_i}$
-

cyclic nucleotide-gated ion channel [24] which possesses C_4 symmetry. Finally, Section 9.6 reports results for the GroEL protein [9]. Technically, GroEL has both a 7-fold cyclic symmetry about some axis, as well as a 2-fold cyclic symmetry (about a different axis which is perpendicular to the above-mentioned axis). Thus, strictly speaking, GroEL has D_7 (dihedral) symmetry. We nevertheless applied Algorithm 4 to it while taking into account only its 7-fold cyclic symmetry (i.e., we treated the molecule as C_7). The code of all algorithms presented in this paper is available as part of the ASPIRE software package [21].

9.1. Implementation details

All tests were executed on a dual Intel Xeon X5560 CPU (12 cores in total), with 96GB of RAM running Linux and an nVidia GTX TITAN GPU. Whenever possible, all 12 cores were used simultaneously, either explicitly using Matlab’s `parfor`, or implicitly, by employing Matlab’s implementation of BLAS, which takes advantage of multi-core computing. Some loop-intensive parts of the algorithm were implemented in \mathbb{C} as Matlab `mex` files. We next describe the discretization of the set $SO_n(3)$ of (29). As implied by Lemma 8.1, any rotation $R \in SO_n(3)$ may be written as $R = R_z(\theta)\tilde{R}$ where (i) \tilde{R} is a rotation matrix whose third row is given by $(\sin \tilde{\theta} \cos \tilde{\phi}, \sin \tilde{\theta} \sin \tilde{\phi}, \cos \tilde{\theta})^T$ for some angles $\tilde{\phi} \in [0, 2\pi)$ and $\tilde{\theta} \in [0, \pi)$, and whose first two rows are set arbitrarily, and (ii) $R_z(\theta)$ is the matrix (15) that rotates a vector by an angle $\theta \in [0, 2\pi/n)$ about the z -axis. As such, we sampled $360,000/n$ evenly-spaced points $(\tilde{\phi}, \tilde{\theta}, \theta)^T \in [0, 2\pi) \times [0, \pi) \times [0, 2\pi/n)$, and formed a matrix $R \in SO_n(3)$ from each such point (we found experimentally that the resulting number of rotations is adequate).

9.2. Complexity analysis

Strictly speaking, the computational complexity of Algorithm 4 is cubic in the number of images due to Algorithm 2. However, in practice, the running time of Algorithm 4 is governed by Algorithm 1, which is quadratic in both the number of images as well as in the size of $SO_n(3)$ of (29). As such, the computational complexity of Algorithm 4 is $\mathcal{O}(m^3 + m^2k^2)$ where k is the number of rotations in the discretization of the set $SO_n(3)$. The space (storage) complexity of Algorithm 4 is $\mathcal{O}(k)$.

As of timing, using a simulated set of $m = 500$ projection-images of a molecule with C_3 symmetry, it took 233 seconds to compute all relative viewing directions v_{ij} , 3.1 seconds to resolve the handedness synchronization, 41 seconds to estimate the in-plane rotation angles, and 601 seconds in order to reconstruct the density map.

9.3. Simulated noisy data

We first tested Algorithm 4 on several datasets of simulated noisy images. Specifically, we generated four sets of m projection-images, with $m = 500, 1000, 1500, 2000$. The projection-images in each set were generated from the three-dimensional density map EMD-6458 [20] (which possesses C_{11} symmetry) available in the Electron Microscopy Data Bank (EMDB) [23]. The orientation R_i of each projection-image was drawn uniformly at random from the uniform distribution on $SO(3)$, and the size of each projection-image was 65×65 pixels. We generated four different copies of each of these sets of projection-images by corrupting the projection-images in each set by an additive Gaussian white noise with $\text{SNR} \in \{1/2, 1/4, 1/8, 1/16\}$, where SNR (signal-to-noise ratio) is defined as the ratio between the energy (variance) of the signal and the energy of the noise.

We then applied Algorithm 4 to each of the resulting sixteen sets of projection-images. For each such set we obtained an estimated set of rotations, which we denote by $\{\tilde{R}_i\}_{i=1}^m$, and we reconstructed the volume using the noisy projection-images and the estimated set of rotations. We next describe how we assessed the degree by which each of these sets of estimated rotations $\{\tilde{R}_i\}_{i=1}^m$ differs from the true rotations $\{R_i\}_{i=1}^m$. To this end, we sampled the Fourier-transform \hat{P}_{R_i} of each projection-image P_{R_i} along the direction vectors $c_i^{(l)} = (\cos 2\pi l/L, \sin 2\pi l/L)$, $l = 0, \dots, L - 1$ where $L = 360$, and then lifted these direction vectors to \mathbb{R}^3 , i.e., we defined $c_i^{(l)} = (\cos 2\pi l/L, \sin 2\pi l/L, 0)$, $l = 0, \dots, L - 1$. We then computed for each pair (i, l) the angle ϵ_{il} between $R_i c_i^{(l)}$ and $\tilde{R}_i c_i^{(l)}$, that is

$$\epsilon_{il} = \arccos \left\langle R_i c_i^{(l)}, \tilde{R}_i c_i^{(l)} \right\rangle, \quad i = 1, \dots, m, \quad l = 0, \dots, L - 1, \quad (61)$$

which measures the error in the estimation of the three-dimensional position of the Fourier ray $c_i^{(l)}$. In addition, the quality of each of the reconstructions was assessed by the resolution obtained using the 0.5 criterion of the Fourier shell correlation (FSC) curve [19] with respect to the reference density map EMD-6458 available in [23]. Table 1 lists the median angular error of ϵ_{il} (over all i and l) for each of the sets along with the obtained resolutions. The table illustrates the robustness of Algorithm 4 to noise as the number m of images increases.

9.4. Trimeric HIV-1 envelope glycoprotein (C_3)

We next tested Algorithm 4 on the Trimeric HIV-1 envelope glycoprotein dataset. The dataset consists of 14199 raw particle images provided in the EMPIAR-10004 dataset [22] from the EMPIAR archive [6]. The raw particle images are of size 127×127 pixels, with pixel size of 2.16\AA . We processed the raw particle images

SNR \ m	1/2	1/4	1/8	1/16
500	2.7° (22.1Å)	5.0° (30.0Å)	9.2° (30.7Å)	13.3° (39.1Å)
1000	3.1° (21.9Å)	6.0° (30.1Å)	5.4° (30.2Å)	14.5° (36.4Å)
1500	2.9° (21.7Å)	4.5° (26.7Å)	5.7° (26.4Å)	9.5° (30.0Å)
2000	2.9° (21.5Å)	4.4° (26.3Å)	6.3° (26.8Å)	8.3° (30.3Å)

Table 1: Median angular estimation errors ϵ_{il} of (61) and obtained resolutions for various levels of noise applied to each of the sets of simulated projection-images.

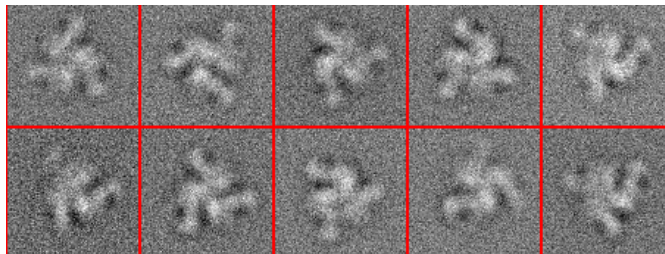


Figure 5: A sample of 89×89 class averages of the EMPIAR-10004 dataset [22] using $K = 100$ raw projection-images per class.

using the ASPIRE [21] software package as follows. First, all images were phase-flipped (in order to remove the phase-reversals in the CTF), down-sampled to size of 89×89 pixels (hence with pixel size of 3.08\AA), and normalized so that the noise in each image has zero mean and unit variance. We next used the class-averaging procedure in ASPIRE [21] to generate class averages from the raw particle images, where each image was averaged with its $K = 100$ most similar images (after proper rotational and translational alignment). Next, we sorted the class averages according to their contrast (i.e., according to the standard deviation of the pixel values of each average). The input to Algorithm 4 was the $m = 2000$ class averages with the highest contrast. A sample of these class averages is displayed in Figure 5.

Next, we applied Algorithm 4 to estimate the rotation matrices $\{\tilde{R}_i\}_{i=1}^m$ that correspond to the m class averages $\{P_i\}_{i=1}^m$. Then, instead of reconstructing the three-dimensional density map using merely the m pairs $\{(\tilde{R}_i, P_i)\}_{i=1}^m$, we made full use of the fact that the underlying molecule is C_3 symmetric by applying the reconstruction to the $3m$ pairs $\{(\tilde{R}_i, P_i), (g_3\tilde{R}_i, P_i), (g_3^2\tilde{R}_i, P_i)\}_{i=1}^m$ (see (8)). Figure 6a displays the reconstructed density map, and Figure 6b displays the reference density map EMD-2484 available in [1] in [23]. The renderings of all volumes in this section were generated using USCF Chimera [12]. The quality of the reconstruction was assessed

using the Fourier shell correlation (FSC) curve [19], implying that the resolution of the model estimated by our algorithm is equal to 21.7\AA according to the 0.5 criterion (Figure 6c).

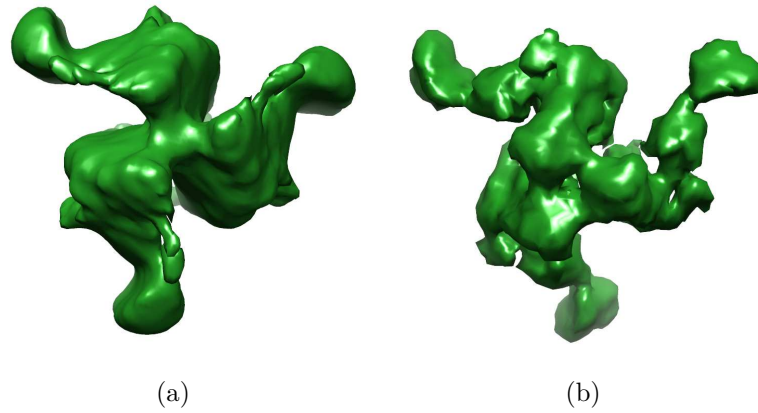
9.5. Human HCN1 hyperpolarization-activated cyclic nucleotide-gated ion channel (C_4)

Next, we applied Algorithm 4 to class averages of the Human HCN1 hyperpolarization activated channel which possesses C_4 symmetry. The class averages were generated from the particle images provided in the EMPIAR-10081 dataset [24]. This dataset comprises of raw particle images of size 256×256 pixels, with pixel size of 1.3\AA . First, the raw particle images were phase-flipped, down-sampled to size of 129×129 pixels, and normalized so that the noise in each image would have zero mean and unit variance. To examine the consistency of Algorithm 4, the raw projection-images were randomly split into two groups of 27,935 images each, and the class-averaging procedure in ASPIRE [21] was used to generate class averages from each of the two groups independently. The class averages were generated by averaging each raw image with its $K = 50$ most similar images (using $K = 100$ resulted later on in inferior results). The input to subsequent steps were the top (highest contrast) $m = 5000$ class averages from each set. A sample of class averages is displayed in Figure 7.

Next, we applied Algorithm 4 to each of these two groups of class averages and estimated the rotation matrices corresponding to each group. We then reconstructed the two density maps using the class averages and the corresponding estimated rotation matrices, while considering the symmetry in the reconstruction process as was described in Section 9.4. The consistency of the reconstructions from the two groups of the data was first assessed using the 0.143 criterion of the FSC curve [19], and was found to be equal to 11.62\AA (Figure 8a). In addition, we compared (using the 0.5 criterion) the reconstructions against the reference density map which was reconstructed from the same dataset as described in [8], and found the resolution to be equal to 14.1\AA (Figure 8b). Figure 9a displays a two-dimensional rendering of a density map generated by Algorithm 4 (only the reconstruction of the first group is shown), and Figure 9b displays a two-dimensional rendering of the reference density map [8].

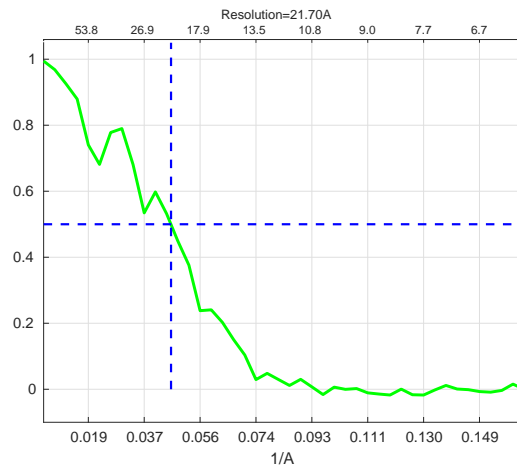
9.6. GroEL protein (D_7 symmetry)

As was already mentioned above, strictly speaking, the GroEL protein [9] has D_7 (dihedral) symmetry, meaning that it has both a 7-fold cyclic symmetry as well as a 2-fold cyclic symmetry. We nevertheless applied Algorithm 4 to it while taking into account only its 7-fold cyclic symmetry. To this end, we used once again



(a)

(b)



(c)

Figure 6: Reconstructed density maps of EMPIAR-10004 [22]. (a) Using Algorithm 4. (b) Reference density map [1]. (c) FSC between the reconstructed density maps.

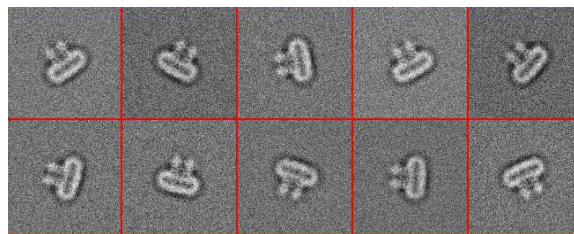


Figure 7: A sample of 129×129 class averages of the EMPIAR-10081 dataset [24] using $K = 50$ raw projection-images per class.

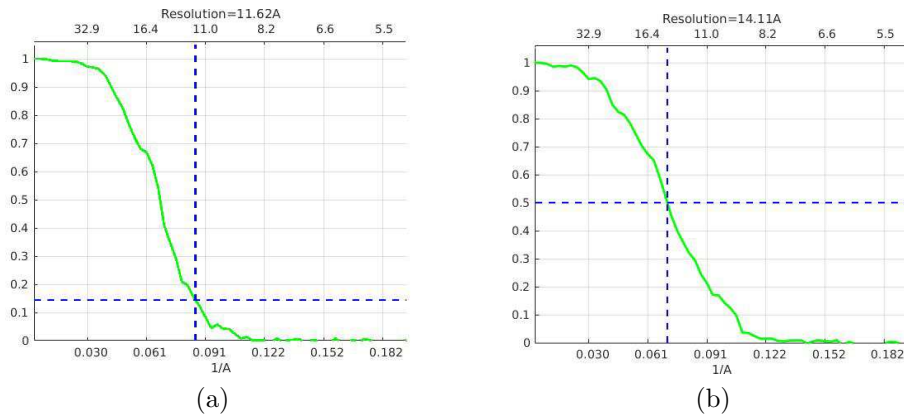


Figure 8: (a) FSC between the density maps reconstructed from the two halves of the data of EMPIAR-10081 [24]. (b) FSC between the density map reconstructed from the first half of the data of EMPIAR-10081 [24] and the reference density map [8].

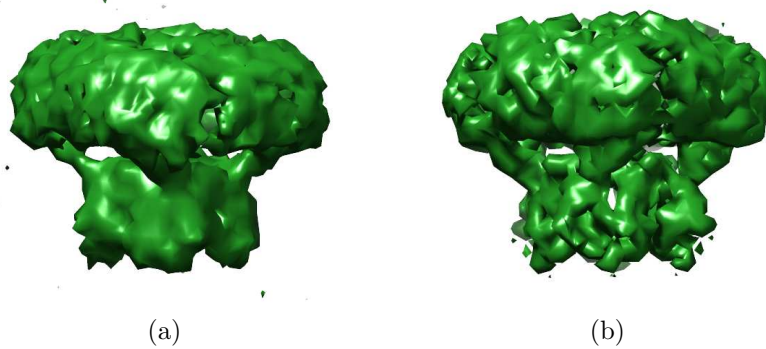


Figure 9: (a) Density map reconstructed from EMPIAR-10081 [24] using Algorithm 4. (b) Reference density map [8].

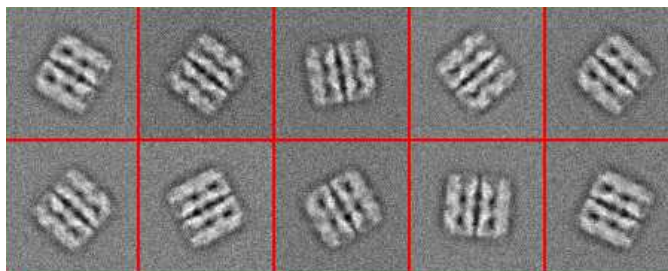


Figure 10: A sample of 89×89 class averages of the GroEL dataset using $K = 100$ raw projection-images per class.

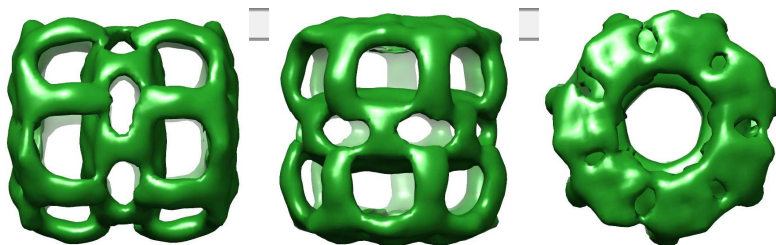


Figure 11: Three different views of the reconstructed density map of the GroEL protein using Algorithm 4.

the class-averaging procedure in ASPIRE [21] to generate class averages from the raw particle images, where each image was averaged with its $K = 100$ most similar images. A sample of class averages is displayed in Figure 10. We then picked the top (highest-contrast) $m = 1000$ class averages, estimated the set of corresponding rotation matrices using Algorithm 4, and reconstructed the density map. The resolution was found to be 5.37\AA (using the 0.5 criterion). Three different views of the reconstructed density map are shown in Figure 11.

10. Discussion and future work

In this paper, we proposed a method for finding the orientations that correspond to a given set of projection-images of a cyclically-symmetric molecule. In addition, we described the inherent geometry that underlies such molecules, as well as the way this geometry is expressed in their projection-images. We further demonstrated the efficacy of our proposed method by providing some numerical results using simulated and experimental datasets.

A typical pipeline for reconstructing a three-dimensional volume from a dataset of

raw particle images consists of first generating a low-resolution model of the molecule from a subset of the dataset, which is then refined to a high-resolution model using the entire dataset. The reason for breaking the reconstruction process into these two steps is that all high-resolution refinement algorithms are based on non-convex optimization schemes (such as the EM-algorithm or stochastic gradient descent) which must be initialized properly in order not to converge to a molecule which is inconsistent with the data. Thus, the first step of the reconstruction pipeline (known as ab-initio reconstruction) should generate a reliable low-resolution model of the molecule. The algorithm presented in this paper addresses this step of the pipeline, and has been shown using experimental data to produce reliable low-resolution models for three different datasets. The resolutions achieved by our algorithm are significantly lower than that of the reference models since our algorithm was applied to only part of the data (in the form of a few hundreds or thousands of class averages), and not to the entire raw data set. Nevertheless, the obtained resolutions are consistent with the required resolutions at the ab-initio modeling step. In particular, high-resolution refinement algorithms typically low-pass filter the ab-initio model, and so any reconstruction whose resolution is better than 30 Å is typically sufficient.

Obviously, all existing software packages include some functionality for ab-initio modelling. However, all of them are based on some local optimization and have no mathematical guarantees. The algorithm presented in this paper is the first to be specifically designed to the geometry of the problem.

A natural future research is to extend the work to other symmetry groups. We are currently at the final stages of devising an algorithm for molecules with D_2 symmetry. As it turns out, the geometry of molecules with D_2 symmetry is completely different from that of molecules with C_n symmetry. The reason is that molecules with D_2 symmetry have three perpendicular symmetry axes, and three corresponding generators of the symmetry group. The resulting algorithm is thus completely different than the one in the current paper. A preliminary analysis of the D_2 algorithm suggests that it may be extended to D_n symmetry with $n > 2$.

Once we derive an algorithm for molecule with D_n symmetry for $n \geq 2$, there remain three symmetry groups to be handled – T (tetrahedral), O (octahedral), and I (icosahedral) symmetries. Those enjoy very high-order symmetry, that should be advantageous due to the large number of common lines between any two images and within each image (self common lines). These high-order symmetry groups are currently under investigation.

Appendices

A. Relative viewing directions estimation for C_3 or C_4 symmetry

In this section, we describe an alternative method for estimating the set of all relative viewing directions $\{v_i v_j^T \mid i \leq j, i, j = 1, \dots, m\}$ which is applicable only to molecules with either C_3 or C_4 symmetry. The following lemma, whose proof is given in Appendix B.4, is central to the proposed method.

Lemma A.1. *For any $n \geq 3$ and for any $i, j \in [m]$ and $s_{ij} \in [n]$,*

$$v_i v_j^T = \begin{cases} \frac{1}{n} \sum_{s=0}^{n-1} \left(R_i^T g_n R_i \right)^s \left(R_i^T g_n^{s_{ij}} R_j \right) \left(R_j^T g_n R_j \right)^s, & (62a) \\ \frac{1}{n} \sum_{s=0}^{n-1} \left(R_i^T g_n^{n-1} R_i \right)^s \left(R_i^T g_n^{s_{ij}} R_j \right) \left(R_j^T g_n^{n-1} R_j \right)^s. & (62b) \end{cases}$$

Similarly, for any $n \geq 3$ and $i \in [m]$,

$$v_i v_i^T = \begin{cases} \frac{1}{n} \sum_{s=0}^{n-1} \left(R_i^T g_n R_i \right)^s, & (63a) \\ \frac{1}{n} \sum_{s=0}^{n-1} \left(R_i^T g_n^{n-1} R_i \right)^s. & (63b) \end{cases}$$

As a result of Lemma A.1 we have the following:

- For $n = 3$, since the only self relative orientations for any $i \in [m]$ are $R_i^T g_n R_i$ and $R_i^T g_n^{n-1} R_i$, and since $(R_i^T g_n R_i)^T = R_i^T g_n^{n-1} R_i$ and vice versa, it follows that in order to recover $v_i v_j^T$ and $v_i v_i^T$ it suffices to determine either one of these two self relative orientation for each $i \in [m]$. To recover $v_i v_j^T$, it is also required to determine a single, arbitrary, relative orientation $R_i^T g_n^{s_{ij}} R_j$.
- For $n = 4$, we shall later show that recovering $R_i^T g_n^2 R_i$ may be easily avoided for any $i \in [m]$. Thus, since for any $i \in [m]$ the only remaining self relative orientations besides $R_i^T g_n^2 R_i$ are $R_i^T g_n R_i$ and $R_i^T g_n^{n-1} R_i$, it follows that in addition to recovering a single, arbitrary, relative orientation $R_i^T g_n^{s_{ij}} R_j$, recovering either one of the remaining two self relative orientations $R_i^T g_n R_i$ or $R_i^T g_n^{n-1} R_i$ for each $i \in [m]$ is sufficient in order to recover any $v_i v_j^T$ and any $v_i v_i^T$.

Applying Lemma A.1 to molecules with C_n symmetry with $n > 4$ requires the estimation of more than just a single self relative orientation per image, and was found to be not robust in practice, and so the method of this section may be applied to either C_3 or C_4 symmetry. The advantage of this method is that it provides more accurate results in practice than the method of Section 6 and is also significantly faster.

A.1. Estimating self relative orientations

We next describe a robust procedure for determining, for both $n = 3$ and $n = 4$, and for every $i \in [m]$, an estimate R_{ii} such that

$$R_{ii} \in \left\{ R_i^T g_n R_i, J R_i^T g_n R_i J, R_i^T g_n^{n-1} R_i, J R_i^T g_n^{n-1} R_i J \right\}. \quad (64)$$

By (23), $R_i^T g_n R_i$ is parameterized by $(\alpha_{ii}^{(1)}, \gamma_{ii}^{(1)}, -\alpha_{ii}^{(n-1)} - \pi)$ and $R_i^T g_n^{n-1} R_i$ is parameterized by $(\alpha_{ii}^{(n-1)}, \gamma_{ii}^{(n-1)}, -\alpha_{ii}^{(1)} - \pi)$. We next show that $\gamma_{ii}^{(1)} = \gamma_{ii}^{(n-1)}$ for any $i \in [m]$. As a result, since by (62a)–(63b) we are oblivious as to which of the self relative orientations in (64) R_{ii} corresponds to, the angles $\alpha_{ii}^{(1)}$ and $\alpha_{ii}^{(n-1)}$ in the aforementioned parameterizations may be freely interchanged. By the projection slice theorem

$$\cos \gamma_{ii}^{(1)} = \left\langle R_i^{(3)}, g_n R_i^{(3)} \right\rangle, \quad (65)$$

$$\cos \gamma_{ii}^{(n-1)} = \left\langle R_i^{(3)}, g_n^{n-1} R_i^{(3)} \right\rangle. \quad (66)$$

Thus, since $g_n^T = g_n^{n-1}$, it follows that $\cos \gamma_{ii}^{(1)} = \cos \gamma_{ii}^{(n-1)}$. As a result, since both of these angles are acute, it follows that indeed $\gamma_{ii}^{(1)} = \gamma_{ii}^{(n-1)}$ (which we subsequently denote by γ_{ii}). In order to recover the angles $\alpha_{ii}^{(1)}$ and $\alpha_{ii}^{(n-1)}$, for which the values along the lines they subtend in \hat{P}_{R_i} are conjugate equal (see (22)), let us define for any $i \in [m]$ the mapping $S_i: (0, \pi) \times (0, 2\pi) \rightarrow \mathbb{R}$ by

$$S_i(\phi, \theta) = \operatorname{Re} \int_{\xi} \hat{P}_{R_i}(\xi \cos \phi, \xi \sin \phi) \hat{P}_{R_i}(\xi \cos \theta, \xi \sin \theta) d\xi, \quad (67)$$

where each ray in \hat{P}_{R_i} is normalized to have its norm equal to one. By (22), the two angles $\alpha_{ii}^{(1)}$ and $\alpha_{ii}^{(n-1)}$ subtend lines in \hat{P}_{R_i} whose Fourier transforms agree up to conjugation. As such, both $(\alpha_{ii}^{(1)}, \alpha_{ii}^{(n-1)})$ and $(\alpha_{ii}^{(n-1)}, \alpha_{ii}^{(1)})$ are solutions of the

optimization problem

$$\begin{aligned} & \text{maximize} && S_i(\phi, \theta) \\ & \text{subject to} && |\phi - \theta| \neq \pi, 0. \end{aligned} \tag{68}$$

The constraint in (68) is needed because any ray through the origin in \hat{P}_{R_i} is conjugate symmetric, and therefore, any two collinear lines would otherwise maximize (68). Moreover, for $n = 4$ this constraint also guarantees that the collinear lines that constitute the second pair of self common lines do not maximize (68). For otherwise, it would lead to estimating $R_i g_4^2 R_i$ instead of the desired $R_i g_4 R_i$ for (62a) and (63a), or $R_i g_4^3 R_i$ for (62b) and (63b).

The main incentive to use self relative orientations is the ability to estimate them in a robust manner due to the following two properties:

1. The domain of each mapping S_i defined in (67) may in fact be restricted to a narrower range of angles. Specifically, we show in Lemma A.2 below that for $n = 3$ it holds that $|\alpha_{ii}^{(n-1)} - \alpha_{ii}^{(1)}| \in [\pi/3, \pi)$, and for $n = 4$ it holds that $|\alpha_{ii}^{(n-1)} - \alpha_{ii}^{(1)}| \in [\pi/2, \pi)$. As such, when the input projection-images are noisy, constraining the optimization problem (68) to these narrower ranges of angles increases the probability of detecting $\alpha_{ii}^{(1)}$ and $\alpha_{ii}^{(n-1)}$.
2. We show in Lemma A.3 below that, for both cases $n = 3$ and $n = 4$, each of the angles γ_{ii} may be computed directly from $|\alpha_{ii}^{(n-1)} - \alpha_{ii}^{(1)}|$. This is in sharp contrast to relative orientations in general, in which the common lines with a third arbitrary central plane are required [16] in order to determine any such angle γ_{ii} . In particular, when the input images are noisy, the common lines with the third image might be misidentified, leading to a wrong estimation of γ_{ii} .

Lemma A.2. *For any $i \in [m]$,*

$$\alpha_{ii}^{(n-1)} - \alpha_{ii}^{(1)} \geq \begin{cases} \pi/3, & \text{if } n = 3, \\ \pi/2, & \text{if } n = 4. \end{cases} \tag{69a}$$

$$\tag{69b}$$

Lemma A.3. For any $i \in [m]$,

$$\cos \gamma_{ii} = \begin{cases} \frac{\cos(\alpha_{ii}^{(n-1)} - \alpha_{ii}^{(1)})}{1 - \cos(\alpha_{ii}^{(n-1)} - \alpha_{ii}^{(1)})}, & \text{if } n = 3, \\ \frac{1 + \cos(\alpha_{ii}^{(n-1)} - \alpha_{ii}^{(1)})}{1 - \cos(\alpha_{ii}^{(n-1)} - \alpha_{ii}^{(1)})}, & \text{if } n = 4. \end{cases} \quad (70a)$$

$$\cos \gamma_{ii} = \begin{cases} \frac{\cos(\alpha_{ii}^{(n-1)} - \alpha_{ii}^{(1)})}{1 - \cos(\alpha_{ii}^{(n-1)} - \alpha_{ii}^{(1)})}, & \text{if } n = 3, \\ \frac{1 + \cos(\alpha_{ii}^{(n-1)} - \alpha_{ii}^{(1)})}{1 - \cos(\alpha_{ii}^{(n-1)} - \alpha_{ii}^{(1)})}, & \text{if } n = 4. \end{cases} \quad (70b)$$

The proof of Lemma A.2 is given in Appendix B.5, and the proof of Lemma A.3 is given in Appendix B.6. Based on (68), on Lemma A.2, and on Lemma A.3, the procedure for determining $\{R_{ii}\}_{i=1}^m$ for molecules with either C_3 symmetry or C_4 symmetry is summarized in Algorithm 5.

Algorithm 5 Recover self relative orientations for molecules with either C_3 symmetry or C_4 symmetry

- 1: **Input:** Images \hat{P}_{R_i} , $i \in [m]$ and symmetry order n (either $n = 3$ or $n = 4$).
 - 2: **if** $n = 3$ **then**
 - 3: **for** $i \in [m]$ **do**
 - 4: $(\alpha_{ii}^{*(1)}, \alpha_{ii}^{*(n-1)}) \leftarrow \arg \max_{|\phi - \theta| \in [\pi/3, \pi]} S_i(\phi, \theta)$ \triangleright (68), (69a)
 - 5: $\gamma_{ii}^* \leftarrow \arccos\left(\frac{\cos(\alpha_{ii}^{*(n-1)} - \alpha_{ii}^{*(1)})}{1 - \cos(\alpha_{ii}^{*(n-1)} - \alpha_{ii}^{*(1)})}\right)$ \triangleright (70a)
 - 6: $R_{ii} \leftarrow R_z(\alpha_{ii}^{*(1)})R_x(\gamma_{ii}^*)R_z(-\alpha_{ii}^{*(n-1)} - \pi)$ \triangleright (15), (23)
 - 7: **end for**
 - 8: **else if** $n = 4$ **then**
 - 9: **for** $i \in [m]$ **do**
 - 10: $(\alpha_{ii}^{*(1)}, \alpha_{ii}^{*(n-1)}) \leftarrow \arg \max_{|\phi - \theta| \in [\pi/2, \pi]} S_i(\phi, \theta)$ \triangleright (68), (69b)
 - 11: $\gamma_{ii}^* \leftarrow \arccos\left(\frac{1 + \cos(\alpha_{ii}^{*(n-1)} - \alpha_{ii}^{*(1)})}{1 - \cos(\alpha_{ii}^{*(n-1)} - \alpha_{ii}^{*(1)})}\right)$ \triangleright (70b)
 - 12: $R_{ii} \leftarrow R_z(\alpha_{ii}^{*(1)})R_x(\gamma_{ii}^*)R_z(-\alpha_{ii}^{*(n-1)} - \pi)$ \triangleright (15), (23)
 - 13: **end for**
 - 14: **end if**
 - 15: **Output:** R_{ii} , $i \in [m]$. $\triangleright R_{ii} \in \{R_i^T g_n R_i, R_i^T g_n^{n-1} R_i, J R_i^T g_n R_i J, J R_i^T g_n^{n-1} R_i J\}$
-

A.2. Estimating relative orientations

In light of Lemma A.1, we next describe how to determine for each of the cases $n = 3$ or $n = 4$, and for every $i < j \in [m]$, a single relative orientation $R_i^T g_n^{s_{ij}} R_j$ where $s_{ij} \in [n]$ is arbitrary, and may be different for each $i < j \in [m]$. To this end, for every two images \hat{P}_{R_i} and \hat{P}_{R_j} , we first determine using normalized cross correlation a single common line between these images. We then find the acute angle between the underlying central planes using the voting scheme [16]. Finally, using (14) we find an estimate R_{ij} for a relative orientation of the central planes, which due to the handedness ambiguity corresponds to either $R_i^T g_n^{s_{ij}} R_j$ or $JR_i^T g_n^{s_{ij}} R_j J$ for some unknown $s_{ij} \in [n]$.

A.3. Local handedness synchronization

At this stage, any two estimates R_{ii} and R_{jj} (obtained by Algorithm 5) satisfy

$$R_{ii} \in \left\{ R_i^T g_n^{s_i} R_i, JR_i^T g_n^{s_i} R_i J \right\}, \quad R_{jj} \in \left\{ R_j^T g_n^{s_j} R_j, JR_j^T g_n^{s_j} R_j J \right\}, \quad (71)$$

for some unknown $s_i, s_j \in \{1, n-1\}$. In light of (63a) and (63b), we therefore set

$$v_{ii} = \frac{1}{n} \sum_{s=0}^{n-1} (R_{ii})^s, \quad i = 1, \dots, m, \quad (72)$$

which guarantees that $v_{ii} \in \{v_i v_i^T, J v_i v_i^T J\}$ for every $i \in [m]$. Similarly to (71), any estimate R_{ij} (obtained in Section A.2) satisfies

$$R_{ij} \in \left\{ R_i^T g_n^{s_{ij}} R_j, JR_i^T g_n^{s_{ij}} R_j J \right\}, \quad (73)$$

for some unknown $s_{ij} \in [n]$. However, in order to find an estimate v_{ij} for $v_i v_j^T$ using either (62a) or (62b), it is essential that (i) $s_i = s_j$ (ii) either all three estimates R_{ii} , R_{jj} , and R_{ij} have a spurious J , or none do at all. In other words, for every $i < j \in [m]$, the task is to manipulate R_{ii} , R_{jj} , and R_{ij} so that they correspond to one of the sets

$$\left\{ \begin{array}{l} R_i^T g_n R_i \\ R_j^T g_n R_j \\ R_i^T g_n^{s_{ij}} R_j \end{array} \right\}, \quad \left\{ \begin{array}{l} R_i^T g_n^{n-1} R_i \\ R_j^T g_n^{n-1} R_j \\ R_i^T g_n^{s_{ij}} R_j \end{array} \right\}, \quad \left\{ \begin{array}{l} JR_i^T g_n R_i J \\ JR_j^T g_n R_j J \\ JR_i^T g_n^{s_{ij}} R_j J \end{array} \right\}, \quad \left\{ \begin{array}{l} JR_i^T g_n^{n-1} R_i J \\ JR_j^T g_n^{n-1} R_j J \\ JR_i^T g_n^{s_{ij}} R_j J \end{array} \right\}, \quad (74)$$

followed by setting

$$v_{ij} = \frac{1}{n} \sum_{s=0}^{n-1} (R_{ii})^s (R_{ij})(R_{jj})^s, \quad (75)$$

as per (62a) and (62b). By so doing, it follows that $v_{ij} = v_i v_j^T$ whenever one of the first two sets in (74) is obtained, and $v_{ij} = J v_i v_j^T J$ whenever one of the last two sets in (74) is obtained. The task of obtaining for every $i < j \in [m]$ either one of the four sets in (74) is referred as the ‘‘local handedness synchronization’’ of the estimates, and will be addressed next. Once this task is completed, we are guaranteed that $v_{ij} \in \{v_i v_j^T, J v_i v_j^T J\}$ for every $i \leq j \in [m]$.

A crucial observation is that both matrices $v_i v_j^T$ and $J v_i v_j^T J$ are rank-1. In addition, if an estimate has a spurious J , e.g., if $R_{ii} = J R_i^T g_n^{s_i} R_i J$, then since $J^2 = I$ it follows that $J R_{ii} J = R_i^T g_n^{s_i} R_i$. Also, if $R_{ii} = R_i^T g_n R_i$, then since $g^T = g_n^{n-1}$, we get that $R_{ii}^T = R_i^T g_n^{n-1} R_i$ and vice versa. Thus, for the case of C_3 (i.e., $n = 3$), we examine for every $i < j \in [m]$, which of the following expressions yields a rank-1 matrix, each obtained by J -conjugating a subset of $\{R_{ii}, R_{jj}\}$, and choosing either R_{ii} (expressions 1-4 in (76)) or R_{ii}^T (expressions 5-8 in (76)).

$$\begin{aligned} 1. & R_{ij} + R_{ii} R_{ij} R_{jj} + R_{ii}^T R_{ij} R_{jj}^T & 5. & R_{ij} + R_{ii}^T R_{ij} R_{jj} + R_{ii} R_{ij} R_{jj}^T \\ 2. & R_{ij} + \mathbf{J} R_{ii} \mathbf{J} R_{ij} R_{jj} + \mathbf{J} R_{ii}^T \mathbf{J} R_{ij} R_{jj}^T & 6. & R_{ij} + \mathbf{J} R_{ii}^T \mathbf{J} R_{ij} R_{jj} + \mathbf{J} R_{ii} \mathbf{J} R_{ij} R_{jj}^T \\ 3. & R_{ij} + R_{ii} R_{ij} \mathbf{J} R_{jj} \mathbf{J} + R_{ii}^T R_{ij} \mathbf{J} R_{jj}^T \mathbf{J} & 7. & R_{ij} + R_{ii}^T R_{ij} \mathbf{J} R_{jj} \mathbf{J} + R_{ii} R_{ij} \mathbf{J} R_{jj}^T \mathbf{J} \\ 4. & R_{ij} + \mathbf{J} R_{ii} \mathbf{J} R_{ij} \mathbf{J} R_{jj} \mathbf{J} + \mathbf{J} R_{ii}^T \mathbf{J} R_{ij} \mathbf{J} R_{jj}^T \mathbf{J} & 8. & R_{ij} + \mathbf{J} R_{ii}^T \mathbf{J} R_{ij} \mathbf{J} R_{jj} \mathbf{J} + \mathbf{J} R_{ii} \mathbf{J} R_{ij} \mathbf{J} R_{jj}^T \mathbf{J} \end{aligned} \quad (76)$$

For example, the first expression in (76) would yield a rank-1 matrix in case $s_i = s_j$ and in addition either all three estimates have a spurious J in them, in which case $v_{ij} = J v_i v_j^T J$, or when none of these estimates have a spurious J in them, in which case $v_{ij} = v_i v_j^T$. The fifth expression in (76) would yield a rank-1 matrix in the same cases as the first expression, only that $s_i \neq s_j$. As another example, consider the case where only R_{ii} has a spurious J in it. Then, the second expression in (76) would yield a rank-1 matrix in case $s_i = s_j$ (otherwise, if $s_i \neq s_j$, then the sixth expression would prevail).

Similarly, due to (71) and (73), in order to use (62a) and (62b) for the case of C_4 (i.e., $n = 4$), we need to examine which of the following eight expressions

$$\frac{1}{4} \sum_{s=0}^3 (J^{\mu_i} \tilde{R}_{ii} J^{\mu_i})^s R_{ij} (J^{\mu_j} R_{jj} J^{\mu_j})^s, \quad \tilde{R}_{ii} \in \{R_{ii}, R_{ii}^T\}, \quad \mu_i, \mu_j \in \{0, 1\} \quad (77)$$

yields a rank-1 matrix. However, it can be shown (see Appendix C) that these eight

expressions are in fact equivalent to

$$\begin{array}{ll}
1. R_{ij} + R_{ii}R_{ij}R_{jj} & 5. R_{ij} + R_{ii}^T R_{ij}R_{jj} \\
2. R_{ij} + \mathbf{J}R_{ii}\mathbf{J}R_{ij}R_{jj} & 6. R_{ij} + \mathbf{J}R_{ii}^T\mathbf{J}R_{ij}R_{jj} \\
3. R_{ij} + R_{ii}R_{ij}\mathbf{J}R_{jj}\mathbf{J} & 7. R_{ij} + R_{ii}^T R_{ij}\mathbf{J}R_{jj}\mathbf{J} \\
4. R_{ij} + \mathbf{J}R_{ii}\mathbf{J}R_{ij}\mathbf{J}R_{jj}\mathbf{J} & 8. R_{ij} + \mathbf{J}R_{ii}^T\mathbf{J}R_{ij}\mathbf{J}R_{jj}\mathbf{J}
\end{array} \tag{78}$$

We thus inspect which of the expressions in (78) results in a rank-1 matrix. Note that in practice, due to misidentification of (self) common lines, it might be that none of the above expressions yields a rank-1 matrix. Therefore, we choose the expression that is closest to be rank-1. Specifically, we first compute the three singular values $s_1^{(k)}, s_2^{(k)}, s_3^{(k)} \in \mathbb{R}$ of each of the expressions $k = 1, \dots, 8$ of (76) for $n = 3$, or of (78) for $n = 4$. Then, we choose the expression k^* such that

$$k^* \leftarrow \arg \min_{k=1, \dots, 8} \left\| \left(s_1^{(k)}, s_2^{(k)}, s_3^{(k)} \right)^T - (1, 0, 0)^T \right\|_2,$$

and decide accordingly whether or not to transpose R_{ii} , whether or not to J -conjugate R_{ii} , and whether or not J -conjugate R_{jj} . Finally, we apply (75) to obtain v_{ij} .

The procedure for finding (for molecules with either C_3 symmetry or C_4 symmetry) all estimates v_{ij} and v_{ii} which, due to the inherent handedness ambiguity, satisfy $v_{ij} \in \{v_i v_j^T, J v_i v_j^T J\}$ and $v_{ii} \in \{v_i v_i^T, J v_i v_i^T J\}$, is summarized in Algorithm 6. This algorithm may replace Algorithm 1 for molecules with either C_3 or C_4 symmetry.

B. Proofs

B.1. Proof of Lemma 3.1

Let $i \in [m]$ and let $s \in [n - 1]$. By (11),

$$(g_n^s R_i)^T q_{ii}^{(s)} = (g_n^s R_i)^T \frac{R_i^{(3)} \times g_n^s R_i^{(3)}}{\left\| R_i^{(3)} \times g_n^s R_i^{(3)} \right\|}. \tag{79}$$

Since $(g_n^s)^T = g_n^{n-s}$, (79) is equal to

$$R_i^T g_n^{n-s} \frac{R_i^{(3)} \times g_n^s R_i^{(3)}}{\left\| R_i^{(3)} \times g_n^s R_i^{(3)} \right\|} = R_i^T \frac{g_n^{n-s} R_i^{(3)} \times R_i^{(3)}}{\left\| R_i^{(3)} \times g_n^s R_i^{(3)} \right\|}. \tag{80}$$

Algorithm 6 Estimate v_{ij} , $i \leq j \in [m]$, for molecules with either C_3 symmetry or C_4 symmetry

- 1: **Input:** (i) images \hat{P}_{R_i} , $i = 1, \dots, m$ (ii) cyclic symmetry order $n = 3$ or $n = 4$.
 - 2: Compute the estimates R_{ii} , $i \in [m]$, using Algorithm 5
 - 3: **for** $i < j \in [m]$ **do**
 - 4: $\alpha_{ij}^*, \alpha_{ji}^* \leftarrow \arg \max_{\phi, \theta \in [0, 2\pi]} \operatorname{Re} \int_{\xi} \hat{P}_{R_i}(\xi \cos \phi, \xi \sin \phi) \overline{\hat{P}_{R_j}(\xi \cos \theta, \xi \sin \theta)} d\xi$ \triangleright (10)
 - 5: Estimate $\gamma_{ij}^* \in [0, \pi)$ using the voting scheme of [16]
 - 6: $R_{ij} \leftarrow R_z(\alpha_{ij}^*) R_x(\gamma_{ij}^*) R_z(-\alpha_{ji}^*)$ \triangleright (14)
 - 7: **end for**
 - 8: **for** $i \in [m]$ **do**
 - 9: $v_{ii} = \frac{1}{n} \sum_{s=0}^{n-1} (R_{ii})^s$ \triangleright (72)
 - 10: **end for**
 - 11: **for** $i < j \in [m]$ **do**
 - 12: $(R_{ii}^*, R_{ij}^*, R_{jj}^*) \leftarrow$ Local handedness synchronization of (R_{ii}, R_{ij}, R_{jj})
 - 13: $v_{ij} = \frac{1}{n} \sum_{s=0}^{n-1} (R_{ii}^*)^s (R_{ij}^*) (R_{jj}^*)^s$ \triangleright (75)
 - 14: **end for**
 - 15: **Output:** v_{ij} , $i \leq j \in [m]$. $\triangleright v_{ij} \in \{v_i v_j^T, J v_i v_j^T J\}$
-

Next, since the cross-product is an anti-symmetric operation, (80) is equal to

$$-R_i^T \frac{R_i^{(3)} \times g_n^{n-s} R_i^{(3)}}{\|R_i^{(3)} \times g_n^s R_i^{(3)}\|} = -R_i^T \frac{R_i^{(3)} \times g_n^{n-s} R_i^{(3)}}{\|R_i^{(3)} \times g_n^{n-s} R_i^{(3)}\|} = -R_i^T q_{ii}^{(n-s)}, \quad (81)$$

where the first equality in (81) is because the vector 2-norm is rotation invariant, and therefore the denominator may be written as

$$\|R_i^{(3)} \times g_n^s R_i^{(3)}\| = \|g_n^s R_i^{(3)} \times R_i^{(3)}\| = \|g_n^{n-s} (g_n^s R_i^{(3)} \times R_i^{(3)})\| = \|R_i^{(3)} \times g_n^{n-s} R_i^{(3)}\|,$$

and the last equality in (81) is due to (11). From (79)–(81) we get that

$$(g_n^s R_i)^T q_{ii}^{(s)} = -R_i^T q_{ii}^{(n-s)}.$$

Thus, from (18),

$$\begin{aligned} \left(\cos \alpha_{gi}^{(s)}, \sin \alpha_{gi}^{(s)}, 0 \right)^T &= - \left(\cos \alpha_{ii}^{(n-s)}, \sin \alpha_{ii}^{(n-s)}, 0 \right)^T \\ &= \left(\cos \left(\alpha_{ii}^{(n-s)} + \pi \right), \sin \left(\alpha_{ii}^{(n-s)} + \pi \right), 0 \right)^T, \end{aligned}$$

from which it follows that

$$\alpha_{gi}^{(s)} = \alpha_{ii}^{(n-s)} + \pi \pmod{2\pi}.$$

□

B.2. Proof of Lemma 6.1

By (4),

$$\frac{1}{n} \sum_{s=0}^{n-1} g_n^{ls} = \frac{1}{n} \sum_{s=0}^{n-1} \begin{pmatrix} \cos \frac{2\pi ls}{n} & -\sin \frac{2\pi ls}{n} & 0 \\ \sin \frac{2\pi ls}{n} & \cos \frac{2\pi ls}{n} & 0 \\ 0 & 0 & 1 \end{pmatrix} = \frac{1}{n} \begin{pmatrix} \sum_{s=0}^{n-1} \cos \frac{2\pi ls}{n} & -\sum_{s=0}^{n-1} \sin \frac{2\pi ls}{n} & 0 \\ \sum_{s=0}^{n-1} \sin \frac{2\pi ls}{n} & \sum_{s=0}^{n-1} \cos \frac{2\pi ls}{n} & 0 \\ 0 & 0 & n \end{pmatrix}. \quad (82)$$

Next, by using the assumption that $(l \bmod n) \neq 0$, we get that

$$\sum_{s=0}^{n-1} \cos \frac{2\pi ls}{n} + i \sum_{s=0}^{n-1} \sin \frac{2\pi ls}{n} = \sum_{s=0}^{n-1} e^{i \frac{2\pi ls}{n}} = \frac{1 - e^{i 2\pi l}}{1 - e^{i \frac{2\pi l}{n}}} = 0.$$

As such,

$$\sum_{s=0}^{n-1} \cos \frac{2\pi ls}{n} = 0, \quad \sum_{s=0}^{n-1} \sin \frac{2\pi ls}{n} = 0,$$

and therefore, the right hand side of (82) is equal to $\text{diag}(0, 0, 1)$, as needed.

□

B.3. Proof of Lemma 8.1

We first prove that given any such R and \tilde{R} , there exists a unique angle $\phi \in [0, 2\pi)$ such that

$$R = R_z(\phi) \tilde{R}. \quad (83)$$

To this end, let us denote the three rows of R by r_1^T, r_2^T, r_3^T , and the three rows of \tilde{R} by $\tilde{r}_1^T, \tilde{r}_2^T, \tilde{r}_3^T$. Since $r_3 = \tilde{r}_3$, it follows that $\tilde{r}_3 \perp r_1$ and $\tilde{r}_3 \perp r_2$, as well as $r_3 \perp \tilde{r}_1$

and $r_3 \perp \tilde{r}_2$. Thus, by direct calculation

$$R\tilde{R}^T = \begin{pmatrix} a & b & 0 \\ c & d & 0 \\ 0 & 0 & 1 \end{pmatrix}, \quad (84)$$

for some $a, b, c, d \in \mathbb{R}$. Since $SO(3)$ is closed with respect to matrix multiplication, it follows that $R\tilde{R}^T \in SO(3)$ as well. As such, there exists a unique angle $\phi \in [0, 2\pi)$ such that

$$R\tilde{R}^T = \begin{pmatrix} \cos \phi & -\sin \phi & 0 \\ \sin \phi & \cos \phi & 0 \\ 0 & 0 & 1 \end{pmatrix}. \quad (85)$$

Finally, by right multiplying (85) by \tilde{R} we get that (since $\tilde{R}^T \tilde{R} = I$),

$$R = R\tilde{R}^T \tilde{R} = \begin{pmatrix} \cos \phi & -\sin \phi & 0 \\ \sin \phi & \cos \phi & 0 \\ 0 & 0 & 1 \end{pmatrix} \tilde{R} = R_z(\phi)\tilde{R}.$$

which proves (83). We next prove (50). Let $n \in \mathbb{N}$, and let $s \in [n]$ be the unique number such that $\frac{2\pi s}{n} + \phi \pmod{2\pi} \in [0, 2\pi/n)$, and further define $\theta = (\frac{2\pi s}{n} + \phi) \pmod{2\pi}$. By construction, $\theta \in [0, 2\pi/n)$. In addition,

$$g_n^s R = g_n^s R_z(\phi)\tilde{R} = R_z\left(\frac{2\pi s}{n} + \phi\right)\tilde{R} \quad (86)$$

$$= R_z\left(\left(\frac{2\pi s}{n} + \phi\right) \pmod{2\pi}\right)\tilde{R} \quad (87)$$

$$= R_z(\theta)\tilde{R}, \quad (88)$$

where (86) follows from (83) and from the fact that $g_n^s = R_z\left(\frac{2\pi s}{n}\right)$, (87) is because $R_z(\tau) = R_z(\tau \pmod{2\pi})$ for any $\tau \in \mathbb{R}$, and (88) uses the definition of θ above. Finally, the uniqueness of θ follows from the uniqueness of ϕ , the uniqueness of s and from (86)–(88). □

B.4. Proof of Lemma A.1

We first prove (62a) and (62b). Let $a \in \{1, n-1\}$ and let $k \in [m]$. Since $R_k R_k^T = I$, we get that $(R_k^T g_n^a R_k)^s = R_k^T g_n^{as} R_k$ for any $s \in [n]$. In addition, since

$\gcd(a, n) = 1$, it follows that a is a generator of \mathbb{Z}_n . As a result,

$$\left\{ \left(R_k^T g_n^a R_k \right)^s \right\}_{s=0}^{n-1} = \left\{ R_k^T g_n^{as} R_k \right\}_{s=0}^{n-1} = \left\{ \left(R_k^T g_n^s R_k \right) \right\}_{s=0}^{n-1}. \quad (89)$$

Thus, for any $i, j \in [m]$ and for any $s_{ij} \in [n]$,

$$\begin{aligned} \frac{1}{n} \sum_{s=0}^{n-1} \left(R_i^T g_n^a R_i \right)^s \left(R_i^T g_n^{s_{ij}} R_j \right) \left(R_j^T g_n^a R_j \right)^s &= \frac{1}{n} \sum_{s=0}^{n-1} \left(R_i^T g_n^s R_i \right) \left(R_i^T g_n^{s_{ij}} R_j \right) \left(R_j^T g_n^s R_j \right) \\ &= \frac{1}{n} \sum_{s=0}^{n-1} R_i^T g_n^s g_n^{s_{ij}} g_n^s R_j \\ &= R_i^T g_n^{s_{ij}} \left(\frac{1}{n} \sum_{s=0}^{n-1} g_n^{2s} \right) R_j. \end{aligned} \quad (90)$$

Since for any $n \geq 3$ it holds that $(2 \bmod n) \neq 0$, applying Lemma 6.1 using $l = 2$ to the right hand side of (90) yields

$$R_i^T g_n^{s_{ij}} \text{diag}(0, 0, 1) R_j = R_i^T \text{diag}(0, 0, 1) R_j = v_i v_j^T,$$

where the first equality used the fact that for any $s_{ij} \in [n]$ the third column of $g_n^{s_{ij}}$ is equal to $(0, 0, 1)^T$, and therefore $g_n^{s_{ij}} \text{diag}(0, 0, 1) = \text{diag}(0, 0, 1)$. This proves (62a) and (62b). We next prove (63a) and (63b). To this end, for both $a = 1$ and $a = n - 1$,

$$\frac{1}{n} \sum_{s=0}^{n-1} \left(R_i^T g_n^a R_i \right)^s = \frac{1}{n} \sum_{s=0}^{n-1} \left(R_i^T g_n^s R_i \right) = R_i^T \left(\frac{1}{n} \sum_{s=0}^{n-1} g_n^s \right) R_i \quad (91)$$

$$= R_i^T \text{diag}(0, 0, 1) R_i = v_i v_i^T, \quad (92)$$

where (91) follows from (89), and (92) follows from Lemma 6.1 using $l = 1$ which indeed satisfies $(l \bmod n) \neq 0$ for any $n \geq 3$. □

B.5. Proof of Lemma A.2

We need first the following two lemmas.

Lemma B.1. For any $n \in \mathbb{N}$, $i \in [m]$, and $s \in [n - 1]$,

$$\left\langle q_{ii}^{(n-s)}, q_{ii}^{(s)} \right\rangle = \frac{\left\langle R_i^{(3)}, g_n^{2s} R_i^{(3)} \right\rangle - \left\langle R_i^{(3)}, g_n^s R_i^{(3)} \right\rangle^2}{1 - \left\langle R_i^{(3)}, g_n^s R_i^{(3)} \right\rangle^2}, \quad (93)$$

where $q_{ii}^{(n-s)}$ and $q_{ii}^{(s)}$ are defined in (11).

Proof. Let $n \in \mathbb{N}$, $i \in [m]$, and $s \in [n - 1]$. By (11)

$$\left\langle q_{ii}^{(n-s)}, q_{ii}^{(s)} \right\rangle = \frac{\left\langle R_i^{(3)} \times g_n^{n-s} R_i^{(3)}, R_i^{(3)} \times g_n^s R_i^{(3)} \right\rangle}{\left\| R_i^{(3)} \times g_n^{n-s} R_i^{(3)} \right\| \left\| R_i^{(3)} \times g_n^s R_i^{(3)} \right\|} = \frac{\left\langle R_i^{(3)} \times g_n^{n-s} R_i^{(3)}, R_i^{(3)} \times g_n^s R_i^{(3)} \right\rangle}{\left\| R_i^{(3)} \times g_n^s R_i^{(3)} \right\|^2}, \quad (94)$$

where the second equality uses the fact that the vector 2-norm is rotation invariant, and therefore

$$\left\| R_i^{(3)} \times g_n^{n-s} R_i^{(3)} \right\| = \left\| g_n^s \left(R_i^{(3)} \times g_n^{n-s} R_i^{(3)} \right) \right\| = \left\| g_n^s R_i^{(3)} \times R_i^{(3)} \right\| = \left\| R_i^{(3)} \times g_n^s R_i^{(3)} \right\|.$$

The nominator in (94) may be simplified by using Lagrange's identity $\langle a \times b, c \times d \rangle = \langle a, c \rangle \langle b, d \rangle - \langle a, d \rangle \langle b, c \rangle$ which holds for any $a, b, c, d \in \mathbb{R}^3$, so that

$$\left\langle R_i^{(3)} \times g_n^{n-s} R_i^{(3)}, R_i^{(3)} \times g_n^s R_i^{(3)} \right\rangle \quad (95)$$

$$= \left\langle R_i^{(3)}, R_i^{(3)} \right\rangle \left\langle g_n^{n-s} R_i^{(3)}, g_n^s R_i^{(3)} \right\rangle - \left\langle R_i^{(3)}, g_n^s R_i^{(3)} \right\rangle \left\langle g_n^{n-s} R_i^{(3)}, R_i^{(3)} \right\rangle$$

$$= \left\langle g_n^{n-s} R_i^{(3)}, g_n^s R_i^{(3)} \right\rangle - \left\langle R_i^{(3)}, g_n^s R_i^{(3)} \right\rangle \left\langle g_n^{n-s} R_i^{(3)}, R_i^{(3)} \right\rangle \quad (96)$$

$$= \left\langle R_i^{(3)}, g_n^{2s} R_i^{(3)} \right\rangle - \left\langle R_i^{(3)}, g_n^s R_i^{(3)} \right\rangle^2, \quad (97)$$

where (96) uses the fact that $\left\langle R_i^{(3)}, R_i^{(3)} \right\rangle = 1$, and (97) is because $(g_n^{n-s})^T = g_n^s$. As for the denominator in (94), since the magnitude of the cross-product is given by the sine of the angle between its arguments, and since $\left\| R_i^{(3)} \right\| = \left\| g_n^s R_i^{(3)} \right\| = 1$, it follows that

$$\left\| R_i^{(3)} \times g_n^s R_i^{(3)} \right\|^2 = 1 - \left\langle R_i^{(3)}, g_n^s R_i^{(3)} \right\rangle^2. \quad (98)$$

Plugging-in (97) and (98) into (94) yields (93) which completes the proof. \square

Lemma B.2. For any $i \in [m]$, let $R_i^{(3)} = (\sin \theta_i \cos \phi_i, \sin \theta_i \sin \phi_i, \cos \theta_i)^T$ be the representation of $R_i^{(3)}$ in spherical coordinates for some $\theta_i \in [0, \pi)$ and $\phi_i \in [0, 2\pi)$. Then,

$$\cos \left(\alpha_{ii}^{(n-1)} - \alpha_{ii}^{(1)} \right) = \begin{cases} \frac{\cos^2 \theta_i - \frac{1}{2} \sin^2 \theta_i}{1 + \cos^2 \theta_i - \frac{1}{2} \sin^2 \theta_i}, & \text{if } n = 3, \\ \frac{\cos^2 \theta_i - 1}{\cos^2 \theta_i + 1}, & \text{if } n = 4. \end{cases} \quad (99a)$$

$$\cos \left(\alpha_{ii}^{(n-1)} - \alpha_{ii}^{(1)} \right) = \begin{cases} \frac{\cos^2 \theta_i - 1}{\cos^2 \theta_i + 1}, & \text{if } n = 4. \end{cases} \quad (99b)$$

Proof. Let $i \in [m]$. For any $n \in \mathbb{N}$, $n > 1$,

$$\cos \left(\alpha_{ii}^{(n-1)} - \alpha_{ii}^{(1)} \right) = \left\langle R_i^T q_{ii}^{(n-1)}, R_i^T q_{ii}^{(1)} \right\rangle = \left\langle q_{ii}^{(n-1)}, q_{ii}^{(1)} \right\rangle \quad (100)$$

$$= \frac{\left\langle R_i^{(3)}, g_n^2 R_i^{(3)} \right\rangle - \left\langle R_i^{(3)}, g_n R_i^{(3)} \right\rangle^2}{1 - \left\langle R_i^{(3)}, g_n R_i^{(3)} \right\rangle^2}, \quad (101)$$

where (100) is due to (18) and because $R_i R_i^T = I$, and (101) is the application of Lemma B.1 with $s = 1$. By (4), we get by a direct calculation that for any $s \in \mathbb{N}$,

$$g_n^s R_i^{(3)} = \left(\sin \theta_i \cos (\phi_i + 2s\pi/n), \sin \theta_i \sin (\phi_i + 2s\pi/n), \cos \theta_i \right)^T,$$

from which it follows that

$$\left\langle R_i^{(3)}, g_n^s R_i^{(3)} \right\rangle = \cos^2 \theta_i + \sin^2 \theta_i \cos (2s\pi/n), \quad \forall s \in \mathbb{N}. \quad (102)$$

We first prove (99a) (i.e., the case $n = 3$). To this end, (100)–(101) become

$$\cos \left(\alpha_{ii}^{(2)} - \alpha_{ii}^{(1)} \right) = \frac{\left\langle R_i^{(3)}, g_3^2 R_i^{(3)} \right\rangle - \left\langle R_i^{(3)}, g_3 R_i^{(3)} \right\rangle^2}{1 - \left\langle R_i^{(3)}, g_3 R_i^{(3)} \right\rangle^2}. \quad (103)$$

Since $g_3^T = g_3^2$ it follows that

$$\left\langle R_i^{(3)}, g_3^2 R_i^{(3)} \right\rangle = \left\langle R_i^{(3)}, g_3^T R_i^{(3)} \right\rangle = \left\langle g_3 R_i^{(3)}, R_i^{(3)} \right\rangle = \left\langle R_i^{(3)}, g_3 R_i^{(3)} \right\rangle.$$

As such, (103) reduces to

$$\begin{aligned} \frac{\langle R_i^{(3)}, g_3 R_i^{(3)} \rangle - \langle R_i^{(3)}, g_3 R_i^{(3)} \rangle^2}{1 - \langle R_i^{(3)}, g_3 R_i^{(3)} \rangle^2} &= \frac{\langle R_i^{(3)}, g_3 R_i^{(3)} \rangle \left(1 - \langle R_i^{(3)}, g_3 R_i^{(3)} \rangle\right)}{\left(1 + \langle R_i^{(3)}, g_3 R_i^{(3)} \rangle\right) \left(1 - \langle R_i^{(3)}, g_3 R_i^{(3)} \rangle\right)} \\ &= \frac{\langle R_i^{(3)}, g_3 R_i^{(3)} \rangle}{1 + \langle R_i^{(3)}, g_3 R_i^{(3)} \rangle}. \end{aligned} \quad (104)$$

Next, applying (102) with $n = 3$ and $s = 1$ gives

$$\langle R_i^{(3)}, g_3 R_i^{(3)} \rangle = \cos^2 \theta_i + \sin^2 \theta_i \cos(2\pi/3) = \cos^2 \theta_i - \frac{1}{2} \sin^2 \theta_i,$$

and plugging this in (104) yields (99a).

We next prove (99b). Applying (102) with $n = 4$ and $s = 1$, and with $n = 4$ and $s = 2$ yields

$$\langle R_i^{(3)}, g_4 R_i^{(3)} \rangle = \cos^2 \theta_i, \quad \langle R_i^{(3)}, g_4^2 R_i^{(3)} \rangle = \cos^2 \theta_i - \sin^2 \theta_i.$$

Plugging this in (101) yields

$$\frac{\cos^2 \theta_i - \sin^2 \theta_i - \cos^4 \theta_i}{1 - \cos^4 \theta_i} = \frac{(\cos^2 \theta_i - 1)(1 - \cos^2 \theta_i)}{(1 + \cos^2 \theta_i)(1 - \cos^2 \theta_i)} = \frac{\cos^2 \theta_i - 1}{\cos^2 \theta_i + 1}, \quad (105)$$

which proves (99b). \square

We are now ready to prove Lemma A.2.

Proof. We begin by proving (69a). Consider the function $f: \mathbb{R} \mapsto \mathbb{R}$ where

$$f(\theta) = \frac{\cos^2 \theta - \frac{1}{2} \sin^2 \theta}{1 + \cos^2 \theta - \frac{1}{2} \sin^2 \theta}, \quad \theta \in \mathbb{R}. \quad (106)$$

Then, in light of (99a), it suffices to show that $\arccos f(\theta) \geq \pi/3$ for any $\theta \in \mathbb{R}$. As it may readily be verified, f is periodic with period π , and therefore $\arccos f$ is periodic with the same period. In addition, $f(\pi/2 + \theta) = f(\pi/2 - \theta)$ for any $\theta \in \mathbb{R}$, see Figure 12a. As a result, it suffices to show that $\arccos f(\theta) \geq \pi/3$ for any

$\theta \in [0, \pi/2]$. To this end, by the chain-rule,

$$\begin{aligned}
\frac{d(\arccos f)}{d\theta} &= \frac{-1}{\sqrt{1-f^2}} \frac{df}{d\theta} = \frac{-1}{\sqrt{1 - \left(\frac{\cos^2 \theta - \frac{1}{2} \sin^2 \theta}{1 + \cos^2 \theta - \frac{1}{2} \sin^2 \theta} \right)^2}} \frac{-3 \sin \theta \cos \theta}{(1 + \cos^2 \theta - \frac{1}{2} \sin^2 \theta)^2} \\
&= \frac{1 + \cos^2 \theta - \frac{1}{2} \sin^2 \theta}{\sqrt{3} \cos \theta} \frac{3 \sin \theta \cos \theta}{(1 + \cos^2 \theta - \frac{1}{2} \sin^2 \theta)^2} \\
&= \frac{\sqrt{3} \sin \theta}{1 + \cos^2 \theta - \frac{1}{2} \sin^2 \theta} \geq 0,
\end{aligned} \tag{107}$$

for any $\theta \in [0, \pi/2]$. As such, $\arccos f$ is non-decreasing in $[0, \pi/2]$. Thus, since $\arccos f$ is continuous, it follows that for any $\theta \in [0, \pi/2]$,

$$\begin{aligned}
\arccos f(\theta) &= \arccos \left(\frac{\cos^2 \theta - \frac{1}{2} \sin^2 \theta}{1 + \cos^2 \theta - \frac{1}{2} \sin^2 \theta} \right) \\
&\geq \arccos \left(\frac{\cos^2 0 - \frac{1}{2} \sin^2 0}{1 + \cos^2 0 - \frac{1}{2} \sin^2 0} \right) \\
&= \arccos \frac{1}{2} = \frac{\pi}{3},
\end{aligned}$$

which proves (69a), see Figure 12a. Similarly, in order to prove (69b), consider the function $g: \mathbb{R} \mapsto \mathbb{R}$ where

$$g(\theta) = \frac{\cos^2 \theta - 1}{\cos^2 \theta + 1}, \quad \theta \in \mathbb{R}. \tag{108}$$

In light of (99b), it suffices to show that $\arccos g(\theta) \geq \pi/2$ for any $\theta \in \mathbb{R}$. Since g is periodic with period π , it follows that $\arccos g$ is periodic with the same period. In addition, $g(\pi/2 + \theta) = g(\pi/2 - \theta)$ for any $\theta \in \mathbb{R}$, see Figure 12b. As a result, it suffices to show that $\arccos g(\theta) \geq \pi/2$ for any $\theta \in [0, \pi/2]$. To this end, by the

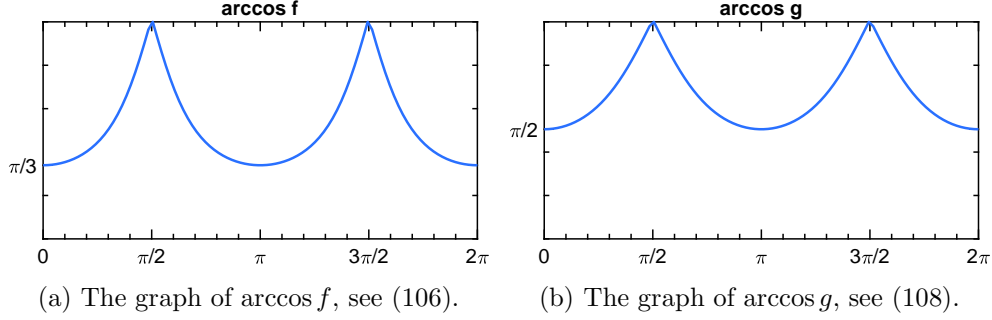


Figure 12: The graphs of the functions used in Lemma A.2.

chain-rule

$$\begin{aligned} \frac{d(\arccos g)}{d\theta} &= \frac{-1}{\sqrt{1-g^2}} \frac{dg}{d\theta} = \frac{-1}{\sqrt{1-\left(\frac{\cos^2 \theta - 1}{\cos^2 \theta + 1}\right)^2}} \frac{-4 \sin \theta \cos \theta}{(\cos^2 \theta + 1)^2} \\ &= \frac{\cos^2 \theta + 1}{2 \cos \theta} \frac{4 \sin \theta \cos \theta}{(\cos^2 \theta + 1)^2} = \frac{2 \sin \theta}{\cos^2 \theta + 1}. \end{aligned}$$

Thus, since $\frac{2 \sin \theta}{\cos^2 \theta + 1} \geq 0$ for any $\theta \in [0, \pi/2]$, we conclude that $\arccos g$ is non-decreasing in $[0, \pi/2]$, and since $\arccos g$ is continuous, it follows that for any $\theta \in [0, \pi/2]$,

$$\arccos g(\theta) = \arccos \left(\frac{\cos^2 \theta - 1}{\cos^2 \theta + 1} \right) \geq \arccos \left(\frac{\cos^2 0 - 1}{\cos^2 0 + 1} \right) = \arccos 0 = \frac{\pi}{2},$$

which proves (69b), see Figure 12b. \square

B.6. Proof of Lemma A.3

Let $i \in [m]$. We begin by proving (70a) (i.e., the case where $n = 3$). It holds that (in fact for any $n \in \mathbb{N}$ and not just for $n = 3$),

$$\cos \left(\alpha_{ii}^{(n-1)} - \alpha_{ii}^{(1)} \right) = \left\langle R_i^T q_{ii}^{(n-1)}, R_i^T q_{ii}^{(1)} \right\rangle = \left\langle q_{ii}^{(n-1)}, q_{ii}^{(1)} \right\rangle \quad (109)$$

$$= \frac{\left\langle R_i^{(3)}, g_n^2 R_i^{(3)} \right\rangle - \left\langle R_i^{(3)}, g_n R_i^{(3)} \right\rangle^2}{1 - \left\langle R_i^{(3)}, g_n R_i^{(3)} \right\rangle^2}, \quad (110)$$

where the first equality in (109) is due to (18), the second equality in (109) is because $R_i R_i^T = I$, and (110) is the result of applying Lemma B.1 with $s = 1$. For $n = 3$, (109)–(110) become

$$\cos(\alpha_{ii}^{(2)} - \alpha_{ii}^{(1)}) = \frac{\langle R_i^{(3)}, g_3^2 R_i^{(3)} \rangle - \langle R_i^{(3)}, g_3 R_i^{(3)} \rangle^2}{1 - \langle R_i^{(3)}, g_3 R_i^{(3)} \rangle^2}. \quad (111)$$

Next, by the projection slice theorem, it follows that

$$\begin{aligned} \langle R_i^{(3)}, g_3 R_i^{(3)} \rangle &= \cos \gamma_{ii}^{(1)} = \cos \gamma_{ii}, \\ \langle R_i^{(3)}, g_3^2 R_i^{(3)} \rangle &= \cos \gamma_{ii}^{(2)} = \cos \gamma_{ii}, \end{aligned} \quad (112)$$

where we have used the fact that $\gamma_{ii}^{(1)} = \gamma_{ii}^{(2)}$ (see text after (66)). Thus, (111) may be written as

$$\cos(\alpha_{ii}^{(2)} - \alpha_{ii}^{(1)}) = \frac{\cos \gamma_{ii} - \cos^2 \gamma_{ii}}{1 - \cos^2 \gamma_{ii}} = \frac{\cos \gamma_{ii}}{1 + \cos \gamma_{ii}}, \quad (113)$$

and solving (113) for $\cos \gamma_{ii}$ yields (70a).

We next prove (70b) (i.e., the case where $n = 4$). Let $i \in [m]$, and let $R_i^{(3)} = (\sin \theta_i \cos \phi_i, \sin \theta_i \sin \phi_i, \cos \theta_i)^T$ be the representation of $R_i^{(3)}$ in spherical coordinates for some $\theta_i \in [0, \pi)$ and $\phi_i \in [0, 2\pi)$. On the one hand, by the projection slice theorem,

$$\cos \gamma_{ii} = \langle R_i^{(3)}, g_4 R_i^{(3)} \rangle. \quad (114)$$

Next, since $g_4 = R_z(\pi/2)$, we get by a direct calculation that

$$g_4 R_i^{(3)} = \left(\sin \theta_i \cos(\phi_i + \pi/2), \sin \theta_i \sin(\phi_i + \pi/2), \cos \theta_i \right)^T,$$

and therefore by a direct calculation it follows that

$$\langle R_i^{(3)}, g_4 R_i^{(3)} \rangle = \cos^2 \theta_i. \quad (115)$$

Thus, from (114) and (115) we get that

$$\cos \gamma_{ii} = \cos^2 \theta_i. \quad (116)$$

On the other hand, by (99b) in Lemma B.2

$$\frac{1 + \cos\left(\alpha_{ii}^{(n-1)} - \alpha_{ii}^{(1)}\right)}{1 - \cos\left(\alpha_{ii}^{(n-1)} - \alpha_{ii}^{(1)}\right)} = \frac{1 + \cos\left(\alpha_{ii}^{(3)} - \alpha_{ii}^{(1)}\right)}{1 - \cos\left(\alpha_{ii}^{(3)} - \alpha_{ii}^{(1)}\right)} = \frac{1 + \frac{\cos^2 \theta_i - 1}{\cos^2 \theta_i + 1}}{1 - \frac{\cos^2 \theta_i - 1}{\cos^2 \theta_i + 1}} = \frac{2 \cos^2 \theta_i}{2} = \cos^2 \theta_i. \quad (117)$$

Equation (70b) now follows from (116) and (117). \square

C. Justification for the expressions in (78)

We prove that the expressions listed in (78) are equivalent to the expressions in (77). To this end, notice that since $g_4^4 = I$, it follows that for any $s_{ij} \in \{0, 1, 2, 3\}$,

$$\begin{aligned} \left(R_i^T g_4 R_i\right)^0 \left(R_i^T g_4^{s_{ij}} R_j\right) \left(R_j^T g_4 R_j\right)^0 &= \left(R_i^T g_4^3 R_i\right)^0 \left(R_i^T g_4^{s_{ij}} R_j\right) \left(R_j^T g_4^3 R_j\right)^0 = R_i^T g_4^{s_{ij}} R_j \\ \left(R_i^T g_4 R_i\right)^1 \left(R_i^T g_4^{s_{ij}} R_j\right) \left(R_j^T g_4 R_j\right)^1 &= \left(R_i^T g_4^3 R_i\right)^1 \left(R_i^T g_4^{s_{ij}} R_j\right) \left(R_j^T g_4^3 R_j\right)^1 = R_i^T g_4^{s_{ij}+2} R_j \\ \left(R_i^T g_4 R_i\right)^2 \left(R_i^T g_4^{s_{ij}} R_j\right) \left(R_j^T g_4 R_j\right)^2 &= \left(R_i^T g_4^3 R_i\right)^2 \left(R_i^T g_4^{s_{ij}} R_j\right) \left(R_j^T g_4^3 R_j\right)^2 = R_i^T g_4^{s_{ij}} R_j \\ \left(R_i^T g_4 R_i\right)^3 \left(R_i^T g_4^{s_{ij}} R_j\right) \left(R_j^T g_4 R_j\right)^3 &= \left(R_i^T g_4^3 R_i\right)^3 \left(R_i^T g_4^{s_{ij}} R_j\right) \left(R_j^T g_4^3 R_j\right)^3 = R_i^T g_4^{s_{ij}+2} R_j. \end{aligned} \quad (118)$$

As such, if for example, $R_{ii} = R_i^T g_4 R_i$ and $R_{jj} = R_j^T g_4 R_j$, or for example, $R_{ii} = R_i^T g_4^3 R_i$ and $R_{jj} = R_j^T g_4^3 R_j$, then setting $\tilde{R}_{ii} = R_{ii}$, and $\mu_i = \mu_j = 0$ in (77), we get using (118) that

$$\frac{1}{4} \sum_{s=0}^3 (J^{\mu_i} \tilde{R}_{ii} J^{\mu_i})^s R_{ij} (J^{\mu_j} R_{jj} J^{\mu_j})^s = \frac{1}{2} \left(R_i^T g_4^{s_{ij}} R_j + R_i^T g_4^{s_{ij}+2} R_j \right) = \frac{1}{2} (R_{ij} + R_{ii} R_{ij} R_{jj}),$$

which is (twice) the first expression in (78). Alternatively, if for example $R_{ii} = R_i^T g_4 R_i$ and $R_{jj} = R_j^T g_4^3 R_j$, or for example $R_{ii} = R_i^T g_4^3 R_i$ and $R_{jj} = R_j^T g_4 R_j$, then by (118), setting $\tilde{R}_{ii} = R_{ii}^T$ and $\mu_i = \mu_j = 0$ in (77) yields (twice) the fifth expression in (78). Other cases are similar and correspond to cases where either R_{ii} has a spurious J , or R_{jj} has a spurious J , or both have a spurious J , in which case setting in (77) (respectively) either $\mu_i = 1$, or $\mu_j = 1$, or $\mu_i = \mu_j = 1$ would yield each of the remaining expressions listed in (78).

Acknowledgments

This research was supported by the European Research Council (ERC) under the European Unions Horizon 2020 research and innovation programme (grant agreement 723991 - CRYOMATH) and by Award Number R01GM090200 from the NIGMS.

References

- [1] Bartesaghi, A, Merk, A., Borgnia, M. J., Milne, J. L. S., and Subramaniam, S. Prefusion structure of trimeric HIV-1 envelope glycoprotein determined by cryo-electron microscopy. Nature structural and molecular biology, 20(12):1352–1357, 2013.
- [2] X. Cheng. Random Matrices in High-dimensional Data Analysis. PhD thesis, Princeton University, 2013.
- [3] Frank, J. Three-Dimensional Electron Microscopy of Macromolecular Assemblies: Visualization of Biological Molecules in Their Native State. Oxford, 2006.
- [4] Goncharov, A. B. Integral geometry and three-dimensional reconstruction of randomly oriented identical particles from their electron microphotos. Acta Applicandae Mathematicae, 11:199–211, 1988.
- [5] Herman, G. T. Fundamentals of Computerized Tomography: Image Reconstruction from Projections. Springer, London, UK, 2nd edition, 2009.
- [6] Iudin, A., Korir, P. K., Salavert-Torres, J., Kleywegt, G. J., and Patwardhan, A. Empiar: a public archive for raw electron microscopy image data. Nature Methods, 13(5):387–388, 2016.
- [7] Z. Kam. The reconstruction of structure from electron micrographs of randomly oriented particles. J. Theor. Biol., 82(1):15–39, 1980.
- [8] Lee, C. and MacKinnon, R. Structures of the Human HCN1 Hyperpolarization-Activated Channel. Cell, 168(1-2):111–120.e11, 2017.
- [9] Ludtke, S. J., Baker, M. L., Chen, D. H., Song, J. L., Chuang, D. T., and Chiu, W. De novo backbone trace of GroEL from single particle electron cryo-microscopy. Structure, 16(3):441–448, 2008.

- [10] F. Natterer. The Mathematics of Computerized Tomography. Classics in Applied Mathematics. SIAM, 2001.
- [11] Natterer, F. and Wübbeling, F. Mathematical Methods in Image Reconstruction. SIAM Monographs on Mathematical Modeling and Computation. SIAM, 2001.
- [12] Pettersen, E. F., Goddard, T. D., Huang, C. C., Couch, G. S., Greenblatt, D. M., Meng, E. C., and Ferrin, T. E. UCSF Chimera—a visualization system for exploratory research and analysis. Journal of Computational Chemistry, 25(13):1605–1612, 2004.
- [13] Pragier, G., Greenberg, I., Cheng, X., Song, J. L., and Shkolnisky, Y. A graph partitioning approach to simultaneous angular reconstitution. IEEE Transactions Computational Imaging, 2(3):323–333, 2016.
- [14] Shkolnisky, Y. and Singer, A. Viewing directions estimation in cryo-EM using synchronization. SIAM Journal on Imaging Sciences, 5(3):1088–1110, 2012.
- [15] Singer, A. , Zhao, Z., Shkolnisky, Y., and Hadani, R. Viewing angle classification of cryo-electron microscopy images using eigenvectors. SIAM Journal on Imaging Sciences, 4(2):723–759, 2011.
- [16] Singer, A., Coifman, R. R., Sigworth, F. J., Chester, D. W., and Shkolnisky, Y. Detecting consistent common lines in cryo-EM by voting. Journal of Structural Biology, 169(3):312–322, 2010.
- [17] J. J. Tuma. Dynamics. New York: Quantum Publishers, 1974.
- [18] Van Heel, M. Angular reconstitution: a posteriori assignment of projection directions for 3D reconstruction. Ultramicroscopy, 21(2):111–123, 1987.
- [19] Van Heel, M. and Schatz, M. Fourier shell correlation threshold criteria. J. Struct. Biol., 151(3):250–262, 2005.
- [20] Zhang, L, Chen, S, Ruan, J, Wu, J, Tong, AB, Yin, Q, Li, Y, David, L, Lu, A, Wang, WL, Marks, C, Ouyang, Q, Zhang, X, Mao, Y, and Wu, H. Cryo-EM structure of the activated NAIP2-NLRC4 inflammasome reveals nucleated polymerization. SCIENCE, (350):404–409, 2015.
- [21] Aspire: Algorithms for Single Particle Reconstruction software package. <http://spr.math.princeton.edu/>.

- [22] Pre-fusion structure of trimeric HIV-1 envelope glycoprotein determined by cryo-electron microscopy. <http://dx.doi.org/10.6019/EMPIAR-10004>.
- [23] Protein Data Bank in Europe-EM resources. <https://www.ebi.ac.uk/pdbe/emdb/>.
- [24] Structures of the Human HCN1 Hyperpolarization-Activated Channel. <http://dx.doi.org/10.6019/EMPIAR-10081>.